5418 *Inorg. Chem.* **2009**, *48*, 5418–5433
DOI: 10.1021/ic900417z

Inorganic Chemistry
Article

Catalytic Dehydrogenation of Ammonia Borane at Ni Monocarbene and Dicarbene Catalysts

Paul M. Zimmerman,* Ankan Paul,† and Charles B. Musgrave‡

Department of Chemical Engineering, Stanford University, Stanford, California 94305. † *Present address: Indian Association for Cultivation of Science, Kolkata, India 70003255.* ‡ *Present address: Department of Chemical and Biological Engineering, University of Colorado at Boulder, Boulder, CO 80309.*

Received March 2, 2009

The development of ammonia borane (**AB**) as a promising hydrogen storage medium depends upon the ability to reversibly release H_2 from the system. We use density functional theory to investigate the mechanism of the catalytic dehydrogenation of **AB** by Ni N-heterocyclic carbene (NHC) complexes, which we show proceeds through Ni monocarbene and dicarbene species. Although $Ni(NHC)_2$ dehydrogenates **AB**, it competitively decomposes into a monocarbene species because **AB** readily displaces NHC from $Ni(NHC)_2$ and reaction of displaced NHC with abundant **AB** makes Ni monocarbene formation thermodynamically favored over the dicarbene catalyst. Prediction of NHC displacement by **AB** is consistent with the experimental observation of NHC-BH_3. The Ni monocarbene species $Ni(NHC)(NH_2BH_2)$ competitively dehydrogenates **AB** with barriers consistent with the experimental temperature required to obtain reasonable reaction rates. The Ni monocarbene pathway also involves rate-limiting steps that exhibit both N−H and B−H kinetic isotope effects (KIEs), as observed experimentally. The predicted N−H and B−H KIEs are also in quantitative agreement with experiment. In contrast, **AB** dehydrogenation by $Ni(NHC)_2$ does not exhibit a B−H KIE. Activation of **AB** at both mono- and dicarbene catalysts proceeds through *cis*-carbene proton acceptance and involves transition states with significant electron delocalization over the π-system of the carbene and its phenyl rings. NHC Ni catalysts involving carbenes with substituent groups containing steric factors that preclude planarity of the phenyl rings to the carbene aromatic system, such as the Imes and Idipp ligands, are predicted to have lower reactivity, in agreement with experiment. The addition of electron donating and withdrawing groups to the phenyl rings demonstrate the importance of π-system electron delocalization by their influence on the barrier to *cis*-carbene proton acceptance.

Introduction

Ammonia borane (**AB**) exhibits several desirable properties required for the chemical storage of hydrogen, including its 19.6 wt % hydrogen content, making it a promising H_2 storage material.[1] However, efficient and reversible H_2 release requires a suitable catalyst.[2] Partial dehydrogenation of **AB** and its analogues by several transition metal catalysts has been demonstrated. For example, titanocene and Ir pincer catalysts have been studied both experimentally and theoretically.[3−6] Baker et al. demonstrated that a homogeneous nickel catalyst with N-heterocyclic carbene (NHC) ligands releases 18 wt % H_2 (>2.5 equiv) from **AB** at 60 °C,[7] an extraordinary amount of H_2 for non-hydrolyzing conditions.[8] Not only does this catalyst release significantly more H_2 from **AB** than other catalysts, it also uses an abundant metal. Enders' carbene (1,3,4-triphenyl-4,5-dihydro-1*H*-1,2,4-triazol-5-ylidene) proved the most effective NHC ligand of the three Baker et al. studied, producing approximately 2.5 equiv of H_2 from **AB**, while the other NHCs produced H_2 at significantly lower rates.[7] The Enders' Ni catalyst was prepared in situ by mixing 2 equiv of Enders' carbene with $Ni(cod)_2$. However, kinetic isotope effect (KIE) measurements result in both B−H and N−H KIEs (ND_3BH_3: 2.3, NH_3BD_3: 1.7, ND_3BD_3: 3.0). This provides important evidence about the nature of the rate-limiting transition states (TS) of the active dehydrogenation mechanism by

*To whom correspondence should be addressed. E-mail: chasm@stanford.edu.

(1) (a) *The Hydrogen Economy: NRC and NAE*; The National Academies Press: Washington, DC, 2004. (b) The Hydrogen Initiative; http://www.aps.org/public_affairs/index.cfm; The American Physical Society, 2004. (c) Basic Research Needs for the Hydrogen Economy; http://www.sc.doe.gov/bes/reports/files/NHE_rpt.pdf; Office of Science at the U.S. DOE, 2004.

(2) (a) Stephens, F. H.; Pons, V.; Baker, R. T. *Dalton Trans.* **2007**, 2613–2626, and references therein. (b) Pun, D.; Lobkovsky, E.; Chirik, P. J. *Chem. Commun.* **2007**, 3297–3299.

(3) Denney, M. C.; Pons, V.; Hebden, T. J.; Heinekey, D. M.; Goldberg, K. I. *J. Am. Chem. Soc.* **2006**, *128*, 12048–12049.

(4) Paul, A.; Musgrave, C. B. *Angew. Chem., Int. Ed.* **2007**, *46*(43), 8153–8156.

(5) Clark, T. J.; Russell, C. A.; Manners, I. *J. Am. Chem. Soc.* **2006**, *128*, 9582–9583.

(6) Luo, Y.; Ohno, K. *Organometallics* **2007**, *26*, 3597–3600.

(7) Keaton, R. J.; Blacquiere, J. M.; Baker, R. T. *J. Am. Chem. Soc.* **2007**, *129*, 1844–1845.

(8) Clark, T. J.; Whittell, G. R.; Manners, I. *Inorg. Chem.* **2007**, *46*, 7522–7527.

Published on Web 05/20/2009

Scheme 1. Simplified Mechanism for the Activation of **AB** in the Ni NHC Catalytic System Described in This Article[a]

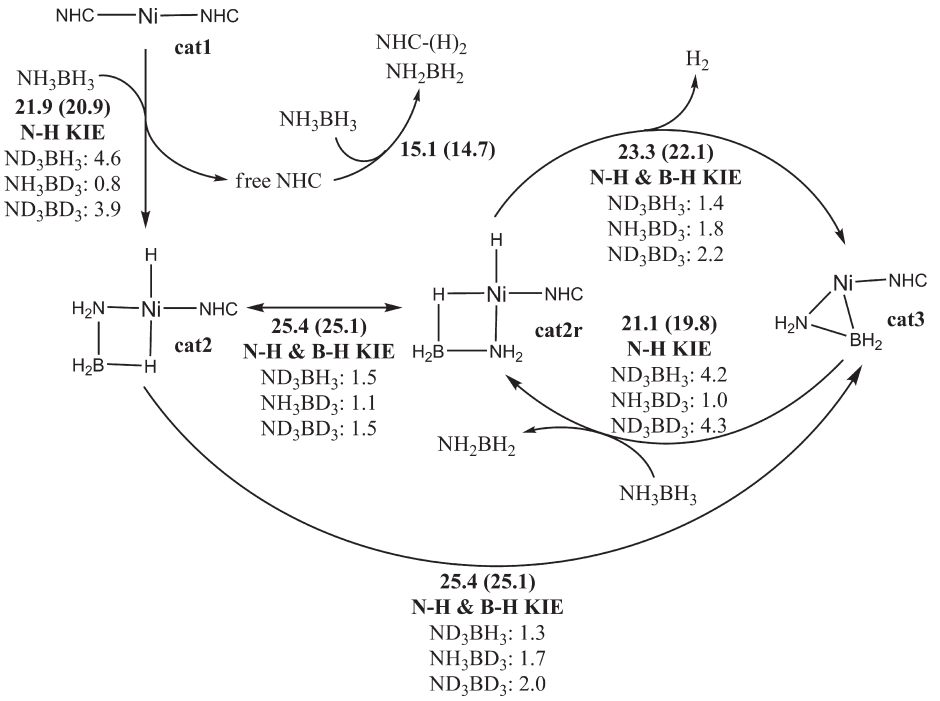

[a] Catalytic cycles of **AB** dehydrogenation at **cat1**, **cat2**, **cat2r**, and **cat3** are described as well as pathways that connect individual cycles by transforming the catalytic Ni species. Reactivity of **free NHC** with **AB** is described elsewhere (see ref 14). Scheme 1 omits inactive pathways and most intermediates for clarity, although these details are shown in related figures and described in the text. See the Supporting Information for a detailed scheme including every energetically feasible pathway and intermediate in this study. The rate limiting steps contain the experimentally observed KIE: ND_3BH_3: 2.3, NH_3BD_3: 1.7, ND_3BD_3: 3.0).[7]

suggesting that they involve significant N−H and B−H motion and possibly dissociation of both N−H and B−H bonds.

The nature of **AB** activation at metal centers is not yet fully understood and varies among different catalysts. **AB** contains both acidic and hydridic hydrogens, creating a variety of possible mechanisms, including stepwise N−H or B−H activation,[6,7,9] and an unusual mechanism in which a metal-bound carbene ligand accepts a proton.[10] Although carbene ligands were originally chosen for the catalyst complex because of their high stability, it is known that not all metal-carbene bonds are inert. For example, ligand displacement has been shown to occur in NHC organometallic systems.[11] Therefore, while the metal-carbene bond in Ni $(NHC)_2$ is strong, **AB** itself could displace an NHC resulting in a complex that may itself be an active catalytic species. For instance, catalytic pathways involving both M(L) and $M(L)_2$ Pd complexes have been observed,[12] indicating that catalysis through both Ni(NHC) and $Ni(NHC)_2$ species may occur in this system. Furthermore, NHC dissociation produces free carbene, which may react with **AB**. The observation of the NHC-BH_3 Lewis Acid−Base complex[7] provides evidence for the presence of free carbene in the reaction medium and motivates the consideration of Ni-monocarbene species formed from the displacement of NHC ligands. In addition, employing cyclohexene as a trap for NH_2BH_2, Baker et al.[13] have shown that NH_2BH_2 remains attached to Ni centers at 25 °C during **AB** activation by Ni NHC catalyst. This result strongly supports this study and our previous study, [14] which both propose that ammonia-borane becomes attached to the Ni catalyst after **AB** activation.

Herein, we report a detailed description of an intricate mechanism for the removal of the first equivalent of H_2 from **AB** at Ni carbene catalysts. First, we analyze the energies of various monocarbene and dicarbene species to determine the thermodynamically feasible intermediates. Next, we investigate the catalytic cycle for **AB** activation at $Ni(NHC)_2$ (**cat1**) and the effect of steric factors and electron delocalization on the reaction energetics. We then describe the pathways for **AB**-assisted NHC displacement from **cat1** and reaction of **free NHC** with **AB**. Next, we report several pathways that produce various monocarbene Ni species (**cat2** and **cat3**) and interconnected pathways for **AB** activation at monocarbene complexes and examine their individual catalytic activities.

Scheme 1 provides an overview of the active pathways described in this article, although several additional reactions were considered, not all are shown in Scheme 1 because they were found to be uncompetitive (see the Supporting Information for a more detailed scheme). Scheme 1 illustrates a catalytic cycle for **AB** dehydrogenation at **cat1** and competitive NHC displacement by **AB** from intermediate **2** to form monocarbene **cat2**. **cat2** does not competitively activate **AB**, but transforms by elimination of H_2 into a second monocarbene species (**cat3**) that does. We consider several

(9) Clark, T. J.; Lee, K.; Manners, I. *Chem. Eur. J.* **2006**, *12*, 8634–8648.
(10) Yang, X.; Hall, M. B. *J. Am. Chem. Soc.* **2008**, *130*(6), 1798–1799.
(11) Crudden, C. M.; Allen, D. P. *Coord. Chem. Rev.* **2008**, *248*, 2247–2273.
(12) Lam, K. C.; Marder, T. B.; Lin, Z. *Organometallics* **2007**, *26*, 758–760.
(13) Pons, V.; Baker, R. T.; Szymczak, N. K.; Heldebrant, D. J.; Linehan, J. C.; Matus, M. H.; Grant, D. J.; Dixon, D. A. *Chem. Commun.* **2008**, 6597.
(14) Zimmerman, P. M.; Paul, A.; Zhang, Z.; Musgrave, C. B. *Angew. Chem., Int. Ed.* **2009**, *48*, 2201.

catalytic **AB** dehydrogenation cycles involving **cat3** herein but describe catalytic pathways involving reactions of both **cat3** and free carbene elsewhere.[14] We show that carbenes displaced from $Ni(NHC)_2$ react with **AB** and do not easily reassociate with Ni-monocarbene species to regenerate Ni $(NHC)_2$. Consequently, dehydrogenation of **AB** shifts from activation by dicarbene Ni to monocarbene Ni. Because production of catalytically active monocarbene species is competitive with **AB** activation by **cat1**, no induction period is expected for monocarbene formation or **AB** dehydrogenation by **cat3**. We provide detailed explanations for the unique reactivity of **AB** and N-heterocyclic carbenes, including the steric, electronic, and entropic effects that influence the kinetics and composition of the reacting system. The predicted KIE values for rate limiting steps agree quantitatively with experiment[7] and support the suggestion that catalytic species other than $Ni(NHC)_2$ must be active in this system.

AB dehydrogenation at **cat1** was recently shown by Hall and co-workers to involve proton transfer to a metal-ligated carbene of $Ni(NHC)_2$.[10] We significantly expand on the description of this mechanism by reporting how the kinetics of this pathway are remarkably sensitive to steric and delocalization factors and by delineating additional intermediates and pathways, including competitive transformation of **cat1** to monocarbene species. Although **AB** activation at **cat1** explains the presence of N−H KIE, it fails to account for the experimentally observed B−H KIE. [see Supporting Information of ref 10] It was suggested that the observed B−H KIE from NH_3BD_3 and ND_3BD_3 results from a kinetic barrier in the removal of a second equivalent of dihydrogen from **AB** (see Supporting Information in ref 10). However, Baker et al. measured the KIE from the disappearance of **AB** (and not aminoborane oligomers representing the second or third equivalents of H_2) using ^{11}B NMR.[7] Therefore, the observed B−H KIE must be present in the rate-limiting transition state for release of the first equivalent of H_2 from **AB** itself without resort to consideration of the second equivalent. Hence, we investigate several additional pathways resulting in the formation of additional Ni species and then determine their ability to catalytically dehydrogenate **AB**. The calculated KIEs of the respective rate-limiting steps of these additional pathways quantitatively account for the observed KIEs in release of the first equivalent of H_2 from **AB**.

Throughout this article, we use the following system for labeling various species: **cat1**, **cat2**, **cat2r**, and **cat3** refer to the most general Ni-dicarbene and Ni-monocarbene complexes for **AB** activation. Numbers (**1** through **7**) refer to intermediates associated with dicarbene Ni (**cat1**), and letters (**A** through **J**) refer to intermediates associated with monocarbene Ni (**cat2**, **cat2r**, and **cat3**). **TSX-Y** refers to transition states connecting the species **X** to **Y**, for instance **TScat2-C** connects **cat2** to species **C** along a pathway confirmed using an intrinsic reaction coordinate (IRC) analysis.

Computational Details. All geometries are optimized using the B3LYP hybrid exchange density functional and a mixed basis set consisting of 6-31++G** on nickel, nickel hydrides, and ammonia borane, and 6-31G* on the NHC ligands as implemented in Gaussian03.[15] IRC calculations are performed for all transition state structures to confirm that they indeed connect the reported intermediates along each pathway. Solution phase corrections to the energies are calculated with the CPCM solvent model.[16] These solvent calculations utilize THF (ε = 7.58) and benzene (ε = 2.25) to represent the experimental mixture of diglyme (ε = 7.23) and C_6D_6, respectively. Solvated zero-Kelvin electronic energies including zero-point energies are reported as energy in THF with zero-point corrected energies in benzene shown in parentheses. The two phenyl rings closest to Ni are included while a single phenyl group is removed from the back of Enders' carbene to reduce computational demand. This approach results in TS structures and corresponding activation barriers that agree quantitatively (within ~1 kcal/mol) with results of using the full catalyst (see Supporting Information). Additional computational details are available in the Supporting Information, including a comparison of B3LYP results with the M05 functional.

Table 1. Relative Energies in kcal/mol of Possible Ni Complexes Referenced to **cat1** and Free Ligands[a]

	E(THF) kcal/mol	*E*(benzene) kcal/mol
$Ni(cod)_2$	16.3	16.9
Ni(NHC)	41.6	45.8
THF-Ni(NHC)	22.2	23.8
benzene-Ni(NHC)	22.7	23.6
η^2 AB-Ni(NHC)	19.6	19.9
cat1: $Ni(NHC)_2$	0.0	0.0
cat2: $Ni(NHC)(NH_2BH_3)H$	0.3	−1.3
cat3: $Ni(NHC)(NH_2BH_2)+H_2$	14.7[b]	12.6[b]

[a] **cat1**, **cat2** and **cat3** are the most energetically stable complexes. [b] When irreversible release of gaseous H_2 is considered, free energy for formation of **cat3** is 6.8 (4.7 kcal/mol). **cat3** formation from **cat2** is essentially irreversible because the $H_{2(g)}$ leaves the system. Monocarbene Ni species are additionally stabilized by the reaction of **free NHC** with **AB** to form NHC-$(H)_2$, as NHC-$(H)_2$ cannot ligate to Ni.

Relative Energies of Potential Monocarbene and Dicarbene Ni Species. Because the active catalytic species was not determined experimentally, [7] complexes other than the initial dicarbene Ni species (**cat1**) may be catalytically active. A comparison of the relative energies of various possible species can determine their thermodynamic accessibility. Several possible nickel complexes could result from the combination of NHC ligands, **AB**, solvent (diglyme, THF, or benzene) together in solution. Table 1 shows the relative energies of several possible Ni complexes. The experimental source of Ni is $Ni(cod)_2$, where cod (1,5-cyclooctadiene) is easily displaced by NHC. Reactivity of $Ni(cod)_2$ is not investigated in this study because it caused only slow **AB** dehydrogenation and was deactivated during the experiment.[7] Without **AB** in the mixture, $Ni(NHC)_2$ (**cat1**) is the most abundant Ni complex because solvent or cod ligation is weak compared to the strong NHC ligation. We calculate the nickel carbene bond strength in $Ni(NHC)_2$ to be 41.6 kcal/mol (45.8 kcal/mol). With **AB** present, however, there are two energetically feasible monocarbene species that could result from displacement of NHC by **AB**. These species,

(15) M. J. Frisch et al. *Gaussian03*, revision E.01; Gaussian, Inc.: Wallingford, CT, 2004. See the Supporting Information for full citation.

(16) Cossi, M.; Rega, N.; Scalmani, G.; Barone, V. *J. Comput. Chem.* **2003**, *24*, 669–681.

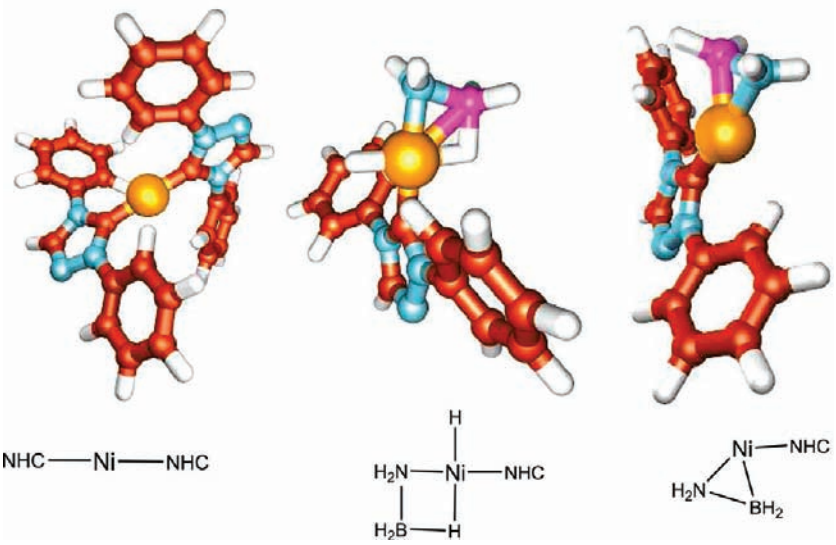

Figure 1. Enders' NHC model Ni catalyst **cat1** (left) and its alternative monocarbene catalysts **cat2** (middle) and **cat3** (right). While **cat1** and **cat2** have nearly identical enthalpies, **cat2** is entropically favored because of dissociation of an **NHC** ligand. Though **cat3** is energetically less stable than **cat1** and **cat2**, production of $H_{2(g)}$ entropically favors **cat3**. Therefore release of H_2 shifts the equilibrium from **cat2** to **cat3**. See Table 1 for a comparison of the relative energies of these species.

Ni(NHC)(H)(NH_2BH_3) (**cat2**) and Ni(NHC)(NH_2BH_2) (**cat3**) are shown in Figure 1 along with **cat1**. In principle, $(NH_2BH_2)_n$ oligomeric species formed from **AB** dehydrogenation could also displace NHC from $Ni(NHC)_2$.[17] During the early phase of catalysis, however, **AB** will be much higher in concentration than oligomeric $(NH_2BH_2)_n$ or $NH_3(NH_2BH_2)_m(BH_3)$ species, which will primarily lead to formation of **cat2** and **cat3** over Ni complexes with oligomers. Hence, we limit our study beyond $Ni(NHC)_2$ to the complexes of Ni(NHC) with **AB**.

The square planar monocarbene Ni(II) complex **cat2** is produced by displacement of NHC from **cat1** by **AB** and is nearly isoenergetic to **cat1** (within the accuracy of the method) with an energy 0.3 kcal/mol (−1.3 kcal/mol) relative to **cat1**. However, **NHC-AB** adduct formation stabilizes **cat2** by 8.0 kcal/mol (11.8 kcal/mol) over **cat1**. **cat2** can be viewed as Ni with one hydride and NH_2BH_3 3-fold coordinated to the Ni via N−B−H, where the nitrogen of NH_2BH_3 donates its lone pair to the metal while the boron end forms an agostic B−H interaction with the metal. This agostic interaction is analogous to Ni-CH_2CH_3 agostic moieties that have been observed in ethylene polymerization schemes.[18,19] Eliminating H_2 from **cat2** produces **cat3**, where NH_2BH_2 is bound to the Ni(0) center. Because NH_2BH_2 is isoelectronic to C_2H_4, the metal to NH_2BH_2 bonding is similar to ethylene's binding to Ni complexes,[20] where ethylene association to Ni has a bond strength of at least 34 kcal/mol in $(C_2H_4)Ni(PH_3)_2$.[21,22] The NH_2BH_2 bond strength in **cat3** of 26.1 kcal/mol (29.0 kcal/mol) is similar, and its structure indicates Ni d-orbital to NH_2BH_2 π-orbital donation causing the B and N to be partly tetrahedral. Although **cat3** is energetically unfavorable with respect to **cat1** (because NH_2BH_2 displacement by **free NHC** is exothermic by 14.7 kcal/mol), reaction of **free NHC** with abundant **AB** forms **NHC-(H)$_2$**, which depletes **free NHC** and shifts the equilibrium toward **cat3**.[14]

Table 2. Rate-Limiting Barrier and KIE for $Ni(NHC)_2$ + AB → $Ni(NHC)_2$ + NH_2BH_2 + H_2 Beginning with Listed Activation

	limiting barrier (kcal/mol)		KIE		
AB activation type	*E* (THF)	*E* (Benzene)	ND_3BH_3	NH_3BD_3	ND_3BD_3
cis N−H activation	28.2	28.5	4.3	0.9	4.1
cis B−H activation[a]	36.5	35.9	6.6	1.2	8.4
trans B−H activation	50.3	51.3	N/A	N/A	N/A
trans concerted activation	32.3	31.8	5.0	0.9	4.6
cis carbene activation (**TS1−2**)	20.9	21.9	4.6	0.8	3.9
experiment			2.3	1.7	3.0

[a] The barrier for *cis* B−H activation is the result of a high N−H activation barrier to complete the cycle.

The energies for the various Ni species reported in Table 1 determine the thermodynamic feasibility of replacing NHC ligands with **AB** and are used to justify limiting the set of species we investigate further. Next, we investigate various pathways for **AB** dehydrogenation catalyzed by the thermodynamically feasible species and for producing these species from the $Ni(NHC)_2$ starting catalyst and **AB** as outlined in Scheme 1. First, we examine the chemistry of the starting catalyst, **cat1**, describe how this species does not exhibit the experimentally observed **AB** B−H KIE and competitively transforms into **cat2** by generating **free NHC**. Following the description of the chemistry of **cat1** we address reactions involving the monocarbene species **cat2** and **cat3**.

(17) (a) Timoshkin, A. Y.; Schaefer, H. F.III *J. Phys. Chem. A* **2008**, *112*, 13180. (b) Timoshkin, A. Y.; Schaefer, H. F.III *J. Phys. Chem. C* **2008**, *112*, 13816.
(18) Leatherman, M. D.; Svejda, S. A.; Johnson, L. K.; Brookhart, M. *J. Am. Chem. Soc.* **2003**, *125*, 3068–3081.
(19) Kogut, E.; Zeller, A.; Warren, T. H.; Strassner, T. *J. Am. Chem. Soc.* **2004**, *126*, 11984–11994.
(20) Albright, T. A.; Hoffmann, R.; Thibeault, J. C.; Thorn, D. L. *J. Am. Chem. Soc.* **1979**, *101*(14), 3801–3812.
(21) Massera, C.; Frenking, G. *Organometallics* **2003**, *22*(13), 2758–2765.
(22) Li, J.; Schreckenbach, G.; Ziegler, T. *Inorg. Chem.* **1995**, *34*(12), 3245–3252.

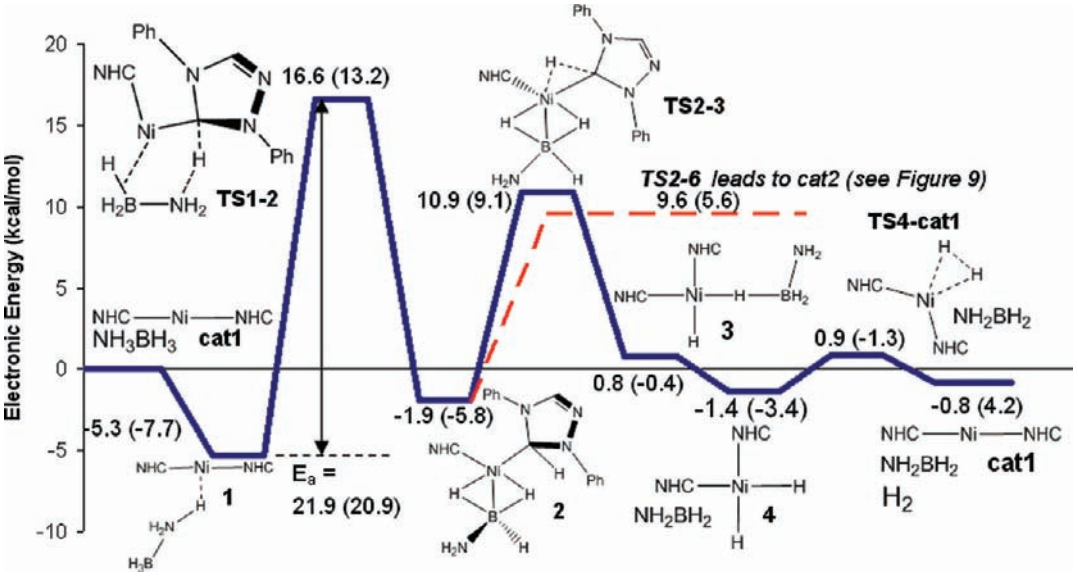

Figure 2. Electronic energies for catalytic dehydrogenation of **AB** at **cat1** proceeding through adduct formation, proton transfer, C−H activation and NH_2BH_2 release, and finally H_2 release. The rate limiting TS does not exhibit significant B−H motion, so this pathway only contains N−H KIE. Figure 9 illustrates the most active pathway for **AB** reaction with **cat1**, which yields monocarbene **cat2**. Below we show **TS2−6** is the lowest energy pathway proceeding through intermediate **2**, which easily transforms to **cat2**.

***cis*-Carbene Activation of AB at the Ni(NHC)$_2$ Catalyst.** Although a variety of mechanisms can potentially dehydrogenate **AB** at **cat1** (see Table 2), the lowest barrier *catalytic* pathway we have found is outlined in Figure 2. However, as shown later, alternative competitive branches from species **2** exist (see Scheme 2). **AB** activation at **cat1** proceeds through an unusual mechanism where **AB** associates to Ni through a bridging acidic hydrogen, which then transfers as a proton to the sp^2 lone pair of a carbene to activate **AB**. In this step (**TS1−2**) one carbene simultaneously acts as a proton acceptor and as a ligand bound to the metal center. This step produces **2**, which is a square-planar complex with NH_2BH_3 attached to the nickel. **2** can then undergo C−H activation to return the carbene to its native state. After NH_2BH_2 dissociates to yield *cis*-Ni(NHC)$_2$(H)$_2$, reductive elimination produces dihydrogen and regenerates the starting catalyst, **cat1**. This pathway includes the proton-accepting carbene and C−H activation steps of Hall's proposed mechanism,[10] but differs significantly in several ways. First, our pathway proceeds through the N−H complex **1**, rather than the higher energy B−H σ-complex. Second, we show that species **4** results from the barrierless dissociation of NH_2BH_2 from **3** and therefore avoids unnecessary reaction steps that eliminate H_2 and NH_2BH_2 to regenerate **cat1**. Additionally, we predict significantly different overall barriers, primarily because of our use of **1** as a lower energy reference energy for the TS.[10] Finally, although this pathway is thermodynamically feasible, we show that more competitive pathways exist that determine the overall reactivity of the Ni NHC system. Specifically, the most favorable pathway involves dissociation of NHC from **cat1** to produce **cat2** (vide infra).

As shown in Figure 2, prior to activation, **AB** forms an N−H complex (**1**) with **cat1** where an acidic hydrogen forms a bridge to the Ni center. This N−H−Ni hydrogen-bonded state is 5.3 kcal/mol (7.7 kcal/mol) below separated **AB** and **cat1** because of the high electron density on the Ni center. An alternative B−H σ-complex lies 8.8 kcal/mol (8.4 kcal/mol) above the N−H complex and 3.5 kcal/mol (0.6 kcal/mol) above **cat1**, although this complex is stable relative to **cat1** in the gas phase. Although the N−H complex **1** is more stable, Hall et al. instead include the unstable B−H σ-complex in their pathway.[10] While the N−H adduct is favored, interchange between the two states can occur by simple dissociation and reassociation.

Scheme 2. Pathways for **AB** Activation at Dicarbene **cat1** Including a Three-Way Branch from **2**[a]

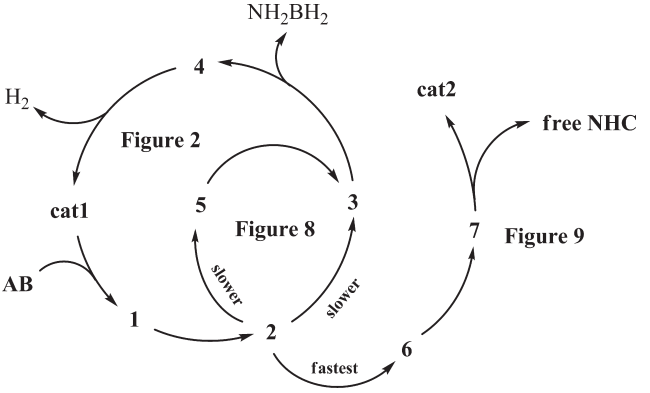

[a] Two branches regenerate **cat1** while the third, and lowest barrier, branch results in **cat2** formation.

Following formation of **1**, **AB** activation passes through the six-member transition state **TS1−2**, shown in Figure 3, in which one carbene accepts a proton from the nitrogen side of **AB** and the two NHC ligands are oriented in a *cis* conformation. **TS1−2** lies 21.9 kcal/mol (20.9 kcal/mol) above **1**. In this TS a single B−H bond donates into the metal center via a σ-complex while the singlet sp^2 carbene carbon hybridizes into an sp^3 center. This change in hybridization leaves an ambiguity regarding the oxidation state of the Ni, which can be described

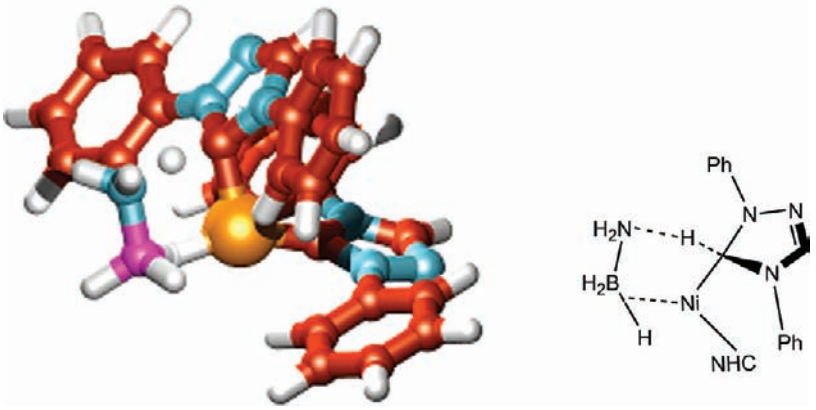

Figure 3. Carbene assisted **AB** activation by proton transfer via **TS1−2**. The phenyl rings are nearly coplanar with the carbene 5-membered ring (see Figure 1).

either as Ni(0) donating a lone pair of electrons into the empty orbital of the cationic carbene carbon or formally oxidized Ni(II) with the pair of electrons now localized on the carbon. To provide insight into this question, we analyzed the electronic structure of **TS1−2** further.

Electronic and Steric Factors of Carbene Protonation. The central 5-membered rings of the carbene ligands form aromatic systems with six π electrons. In normal ligation, the empty p-orbital of the ligating carbon is part of this aromatic system while the carbon sp^2 lone pair is donated to the Ni center. An intriguing aspect of the transformation of **1** into **2** is that at **TS1−2** the active NHC changes its mode of ligation: the NHC no longer donates its lone pair to Ni, changes its hybridization from sp^2 to sp^3, and simultaneously accepts a proton from **AB**. Electron back-donation from the Ni center to the carbene allows the **AB** proton to accept electron density from the carbene lone pair. The increase in electron density on Ni caused by ligation with the electron-rich B−H bond facilitates the back-donation and consequently, the proton transfer. Therefore, the Ni−C bonding interaction and addition of electron density from the associated boron hydride moiety to Ni contribute to the stability of **TS1−2** (overall, the electron density migration is B−H → Ni → C → proton). More importantly, the TS structure of **TS1−2** exhibits phenyl rings nearly coplanar with the central 5-membered ring of NHC, indicating that extended electron delocalization stabilizes this TS and compensates for the loss of carbene ring aromaticity. The highest occupied molecular orbital (HOMO) of **TS1−2**, shown in Figure 4, clearly exhibits participation of the extended carbene π-system, including the phenyl rings, in stabilizing the disruption in aromaticity at the ligating carbon. This characteristic of the electronic structure of **TS1−2** strongly indicates that delocalization over the ligand π-system influences the TS energy and that steric or electronic effects of carbene substituent groups that modify electron delocalization within the π-system will affect the barrier for **TS1−2**.

The effect of π-system delocalization was studied by replacing hydrogens on the phenyl rings of Enders' carbene with NO_2 and NH_2 groups. Electron withdrawing groups such as NO_2 should increase delocalization of π-electron density of the participating NHC and

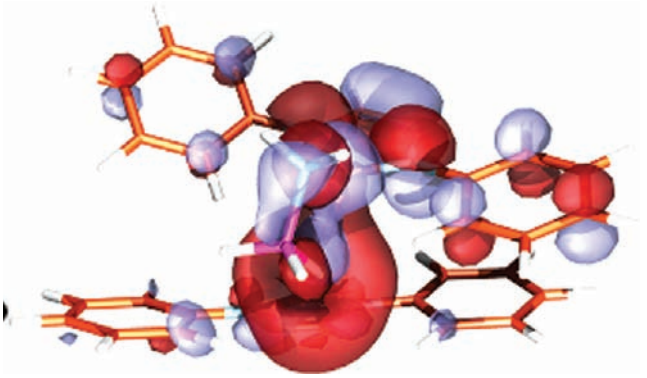

Figure 4. HOMO of **TS1−2** (Figures 2 and 3) showing delocalization of the extended π−system (contribution from the phenyl rings) stabilizing the broken 5-membered ring aromaticity.

decrease the barrier for **TS1−2** if delocalization over the π-system compensates for the break in aromaticity of the carbene 5-membered ring. In fact, the calculated barrier decreases by 5.1 kcal/mol (4.9 kcal/mol) upon addition of an NO_2 group to each phenyl ring of the carbene. In contrast, replacing the hydrogens of the phenyl rings with electron donating groups, such as NH_2, should increase the barrier of **TS1−2** and in fact does lead to higher electron density in the π-system and a concomitant increase in the barrier by 1.8 kcal/mol (1.4 kcal/mol). To ensure that the stabilization of **TS1−2** by π-delocalization is not particular to the B3LYP density functional, we optimized the geometries for **TS1−2** and **1** with the B3PW91, MPW1PW91, and KMLYP functionals. These functionals produce geometries very similar to B3LYP and reproduce the coplanarity between the phenyl rings and the carbene 5-membered ring. The energetic barriers for **TS1−2** with these functionals are slightly lower (by 3.0−4.2 kcal/mol) than B3LYP, indicating that B3LYP is not overestimating the feasibility of **TS1−2** (see Supporting Information). The importance of delocalization of π electron density is further confirmed by analysis of the Imes catalyst activation.

TS1−2 was also studied with the Imes NHC (*N*,*N*′-bis (2,4,6-trimethylphenyl)imidazol-2-ylidene) catalyst, which experimentally dehydrogenated **AB** at a slower

rate than the less bulky Enders' NHC catalyst.[7] We calculate a barrier for the Imes activation via **TS1−2** of 36.5 kcal/mol (36.2 kcal/mol), significantly higher than that of the Enders' model catalyst, indicating that the steric bulk of the Imes carbene raises the barrier for activation. In this case, the methyl groups on the Imes phenyl rings prevent them from taking the coplanar conformation that is possible with the Enders' carbene. Consequently, these methyls indirectly disrupt the extended π-delocalization over the rings. Consistent with this interpretation and in contrast to the Enders' model carbene catalyst, the HOMO of the Imes catalyst at **TS1−2** shows no phenyl π-orbital participation because of their perpendicular orientation with respect to the central 5-membered ring of the NHC (see Supporting Information). The steric hindrance of the Imes methyl groups prevents stabilization of the TS by π-system delocalization, causing **TS1−2** to be energetically unfavorable. This result is in contrast to previous work which used a model for the Imes catalyst that omits the methyl groups of the phenyl rings, thus precluding the steric effect that governs this reaction.[10]

An alternative pathway to the *cis*-carbene proton transfer involves concerted activation (**TS1−4**, Figure 5) of both hydridic and acidic hydrogen to yield *cis*-Ni(NHC)$_2$(H)$_2$ (**4**) and free NH_2BH_2. Unlike **TS1−2**, **TS1−4** at the Imes catalyst is not destabilized by steric factors, making it favored by 5.0 kcal/mol (4.9 kcal/mol) over Imes **TS1−2**. However, the 31.5 kcal/mol barrier of **TS1−4** (Figure 5) for the Imes catalyst still entails a considerably higher barrier than the 21.9 kcal/mol barrier for **TS1−2** of Enders' carbene. The structure of **TS1−4** is somewhat similar to that of **TS1−2**, except that the proton adds to the Ni center rather than to the carbene and the carbene maintains its Ni−C coordinate bond to Ni. Although activation of **AB** at Ni(NHC)$_2$ complexes explains only part of the mechanism under consideration, these results indicate why the Imes system dehydrogenates **AB** at a slower rate than Enders' catalyst. Similarly, the steric bulk of the Idipp NHC (*N*,*N*′-bis(2,6-diisopropylphenyl)imidazol-2-ylidene) catalyst explains its significantly lower rate of **AB** dehydrogenation relative to Enders' Ni NHC. Although **TS1−4** is favorable for the Imes catalyst, a similar TS for concerted addition of hydrogen does not exist with the model Enders' NHC catalyst. Repeated attempts to determine a TS structure for concerted addition at Enders' **cat1** all converged to **TS1−2**.[23]

Completing the *cis*-Carbene Activation Cycle at Ni(NHC)$_2$. As the activated model of Enders' complex proceeds through **TS1−2** toward **2** the carbene withdraws additional electron density from Ni, which causes the boron hydrides to compensate by associating and donating electron density to Ni. The reaction coordinate from **TS1−2** to **2** shows this effect as the geometry and electronic structure evolve to the product with BH_3NH_2

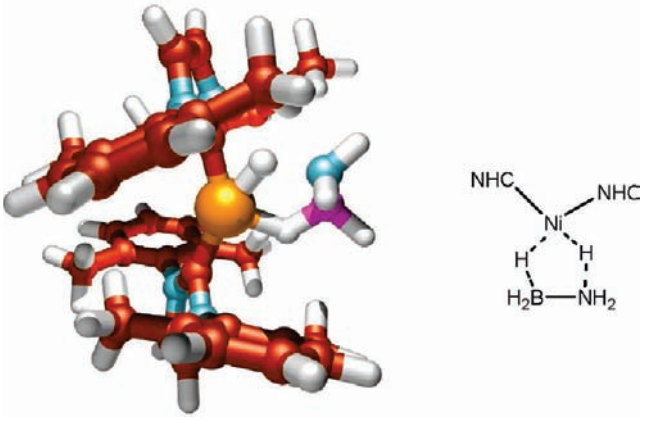

Figure 5. Transition state (**TS1−4**) for concerted activation of **AB** at Imes catalyst. The sterics of the methyls on the phenyl rings restrict them to being nearly orthogonal to the central carbene ligand, preventing extended delocalization of the carbene π-system. This steric effect limits the activity **TS1−2** within the Imes system.

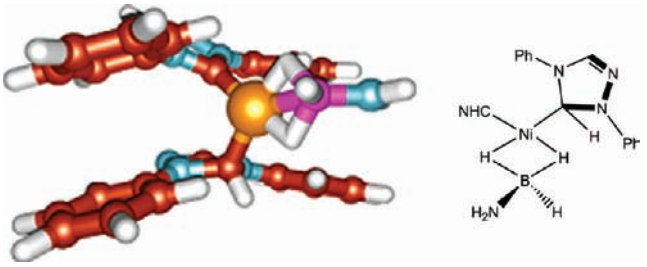

Figure 6. η^2 Ni complex **2** involving double B−H−Ni bridges. An IRC analysis confirms **2** results from **TS1−2**. **2** is less stable than its isomers **5** and **6**, shown in Figures 7 and 10. Figures 2 and 8 show competing energetic profiles involving transformations of **2**.

attached to the Ni of **2** and an **AB** proton now bound to the carbene (Figure 6). Intermediate **2** lies 3.4 kcal/mol (1.9 kcal/mol) above **1** and consists of an unusual H−B−H η^2 attachment to the nickel, similar to the H−B−H η^2 association observed in organometallic complexes such as stable BH_4 adducts to Group 5 metals,[24] and η^2 silyl adducts to group 9 metals.[25] The square planar geometry of **2** indicates that this state is formally 16 electron Ni(II) when counting each B−H association as a two electron ligand. The Mulliken charges on the Ni indicate that Ni is partially oxidized from Ni(0) in **TS1−2** and **2**, with the charge on Ni increasing by 0.29e from **1** to **TS1−2** and by 0.26e from **1** to **2**. The corresponding changes in charge on the activating carbon are −0.31e from **1** to **TS1−2**, and −0.29e from **1** to **2**, indicating the charge donation of Ni to the carbon center. Because the square planar geometry of **2** suggests a formal charge assignment of Ni(II) to **2**, the similar Mulliken charges on Ni for **2** and **TS1−2** imply **TS1−2** is also Ni(II).

We next examine a number of possible reactions involving **2** (see Scheme 2). Figure 2 illustrates the pathway involving C−H activation of **2** through **TS2−3** that yields *cis*-Ni(NHC)$_2$(BH_3NH_2)(H) (**3**) and restores the original **cat1**-type ligation of NHC to the Ni. **TS2−3** lies 12.8 kcal/mol (14.9 kcal/mol) above **2**. This unusually low barrier for C−H

(23) We were, however, able to obtain a stationary point for concerted activation at simplified Enders' **cat1** with the 6-31G* basis set where the lack of polarization functions on the hydrogen modified the potential energy surface such that a concerted activation TS structure exists. However, this pathway is not competitive as single-point energy calculations with the larger basis set at this geometry show that the TS is 10.0 kcal/mol (10.0 kcal/mol) higher in energy than **TS1−2**.

(24) Conway, S. L. J.; Doerrer, L. H.; Green, M. L. H.; Leech, M. A. *Organometallics* **2000**, *19*, 630–637.

(25) Ayed, T.; Barthelat, J-C.; Tangour, B.; Pradere, C.; Donnadieu, B.; Grellier, M.; Sabo-Etienne, S. *Organometallics* **2005**, *24*, 3824–3826.

activation at Ni results from the unstable η^2 attachment of NH_2BH_3 to Ni in **2**. As Figure 2 illustrates, NH_2BH_2 dissociates from **3** to form *cis*-Ni(NHC)$_2$(H)$_2$ (**4**) without forming new bonds. Despite the formation of no new bonds, this step is exothermic by 2.1 kcal/mol (3.0 kcal/mol) and essentially barrierless with the absence of a barrier confirmed using a linear transit scan over increasing Ni−B distances (see Supporting Information). Next, **4** reductively eliminates H_2 via **TS4−cat1** to regenerate **cat1** and release free H_2 with **TS4−cat1** lying only 2.2 kcal/mol (2.1 kcal/mol) above the dihydride **4**. Therefore, as Figure 2 shows, the rate limiting step for catalytic dehydrogenation of **AB** by **cat1** is **TS1−2**. The pathway presented in Figure 2 differs qualitatively from the pathway reported in ref 10 after intermediate **3** because ref 10 does not show the barrierless and exothermic dissociation of NH_2BH_2 from **3** to yield **4**, but instead reports a pathway proceeding from **3** to produce NH_2BH_2 and H_2 with three barriers, the largest of which is 10.6 kcal/mol, substantially above the pathway we report. However, we show below that neither pathway through **3** is competitive with an alternative route branching from **2** that proceeds through **TS2−6**, **TS6−7**, and **TS7−cat2**, as shown in Figure 9.

Because **2** has a dangling NH_2 lone pair we investigated alternative attachments of NH_2BH_3 that are not directly connected along the reaction coordinate illustrated in Figure 2. Figure 8 shows an alternative route from **2** to **3** through **5** where in addition to direct C−H activation via **TS2−3**, **2** can isomerize to the agostic complex **5** shown in Figure 7. This step (**TS2−5**) occurs with a barrier of 14.6 kcal/mol (14.5 kcal/mol) above **2**, making it competitive with **TS2−3**. Complex **5** is 8.6 kcal/mol (8.5 kcal/mol) more stable than **2** because the nitrogen lone pair donation is favored over the weaker η^2 donation of the B−H bonds of **2**. This is consistent with the change in Mulliken charge on Ni of −0.14e from **2** to **5**, indicating that additional charge is donated to the Ni center by the nitrogen. **5** resembles species with agostic interactions seen in analogous hydrocarbon systems[18,19,30] and can transform to **3** through C−H activation of the carbene hydrogen (**TS5−3**) with a barrier of 22.1 kcal/mol (23.0 kcal/mol), which is competitive with **TS2−3**. Conversion of **2** to **3** through intermediate **5** therefore involves an overall barrier slightly higher than **TS1−2** because of the stability of species **5**. The energetic profile containing a comparison of the steps from **2** to **3** is shown in Figure 8.

Is *cis*-Carbene Activation at Ni(NHC)$_2$ the Experimental Mechanism?. The protonation of the carbene via **TS1−2** and C−H activation via **TS2−3** should not be completely unexpected. NHCs are strong bases, with high pK_a values,[26,27] making them well suited to accept protons. Although **TS1−2** is more complicated than simple proton acceptance by unligated carbene, this indicates that the NHC lone pair may be able to accept protons even while partially bound to a metal center. In addition, C−H activation of a carbene proton through **TS2−3** or **TS5−3** is analogous to catalyst formation by adding

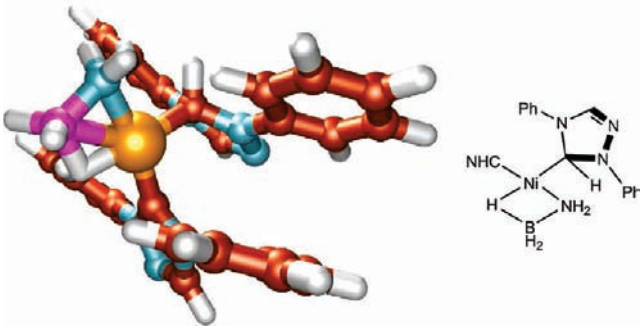

Figure 7. Agostic intermediate **5**, the result of low barrier isomerization of **2** to a more stable species donating a nitrogen lone pair to Ni. Complexes such as **5** are analogous to β-agostic complexes seen in Ni catalyzed olefin polymerization. Here, the Ni-NH_2BH_3 agostic moiety takes the place of the Ni-CH_2CH_3 agostic interaction (see Figure 8).

NHC-(H)$^+$ salts to metals in solution, consistent with the recognized pathway for creating M(NHC) complexes by oxidative addition of a NHC-(H)$^+$ to a transition metal.[27] In fact, experiments have specifically demonstrated oxidative addition of NHC-(H)$^+$ to Ni(0) for this system.[28] Furthermore, combined experimental and theoretical studies have shown Group 10 metals undergoing NHC-(H)$^+$ and NHC-(CH$_3$)$^+$ oxidative addition steps that mirror the C−H activations studied herein.[29−32]

The overall energetic barrier of 21.9 kcal/mol (20.9 kcal/mol) for the *cis*-carbene cycle via **TS1−2** and **TS2−3**, or slightly higher barrier path through **TS1−2**, **TS2−5**, **TS5−3**, implies that this mechanism is feasible at 60 °C. Hall et al. predict a rate limiting free energy barrier of 11.9 kcal/mol,[10] considerably lower than expected considering the reaction conditions. The free energy barrier for **TS1−2** in our study is 25.8 kcal/mol (24.8 kcal/mol). In comparison, in Ohno's study a titanocene catalyst dehydrogenated the **AB** analogue Me_2NHBH_3 at room temperature with an overall free energy barrier of 22.9 kcal/mol [6] and our group reported the energetic barrier for fast **AB** dehydrogenation at an Ir pincer catalyst to be 20.7 kcal/mol.[4] Consequently, our reported overall barrier is consistent with the experimental conditions. The *cis*-carbene cycle exhibits a strong KIE for amine hydrogens, but not for borane hydrogens (ND_3BH_3: 4.6, NH_3BD_3: 0.8, ND_3BD_3: 3.9) because the normal modes corresponding to the rate limiting steps do not involve significant motion of the borane hydrogens. This is in agreement with Hall's study, which showed only N−H KIE for **AB** activation at Ni(NHC)$_2$ (in the Supporting Information of ref 10). Because only N−H KIE is exhibited in this mechanism, further pathways must be active to explain the experimentally observed B−H KIE.

Although **TS1−2** is the lowest barrier transition state for **AB** activation we have found, we have also investigated N−H, B−H, and concerted addition mechanisms at **cat1** with

(26) Alder, R. W.; Allen, P. R.; Williams, S. J. *J. Chem. Soc., Chem. Commun.* **1995**, 1267–1268.
(27) Kim, Y. J.; Streitwieser, A. *J. Am. Chem. Soc.* **2002**, *124*, 5757–5761.
(28) Herrmann, W. A.; Kocher, C. *Angew. Chem., Int. Ed.* **1997**, *36*(18), 2162–2187.
(29) Clement, N. D.; Cavell, K. J.; Jones, C.; Elsevier, C. J. *Angew. Chem., Int. Ed.* **2004**, *43*(10), 1277–1279.
(30) Normand, A. T.; Hawkes, K. J.; Clement, N. D.; Cavell, K. J.; Yates, B. F. *Organometallics* **2007**, *26*, 5352–5363.
(31) McGuinness, D. S.; Cavell, K. J.; Yates, B. F.; Skelton, B. W.; White, A. H. *J. Am. Chem. Soc.* **2001**, *123*, 8317–8328.
(32) McGuinness, D. S.; Cavell, K. J.; Yates, B. F. *Chem. Commun.* **2001**, 355–356.

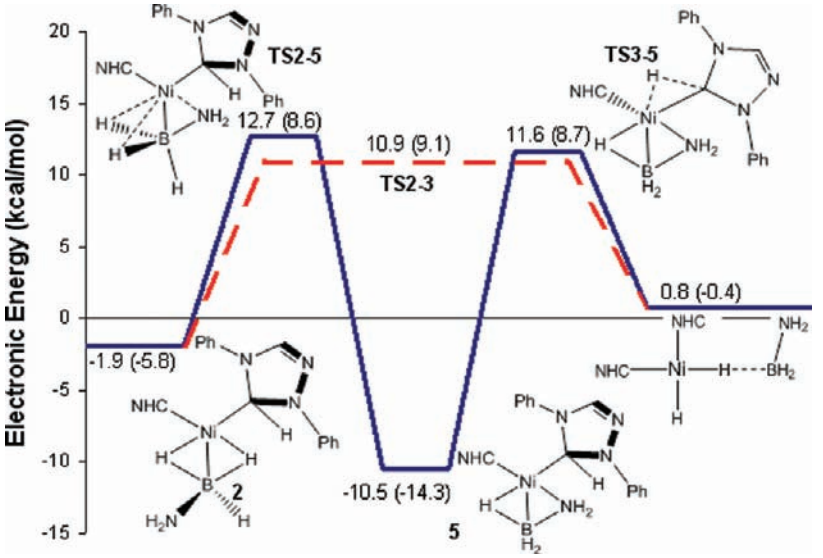

Figure 8. Electronic energy profile of the competing path for transformation of **2** to **3** via isomerization **TS2**−**5** and C−H activation **TS5**−**3**. The barrier of the competing single-step pathway from **2** to **3** (displayed in Figure 2) is represented by the dashed line. An even lower barrier path than these two competing pathways is shown in Figure 9.

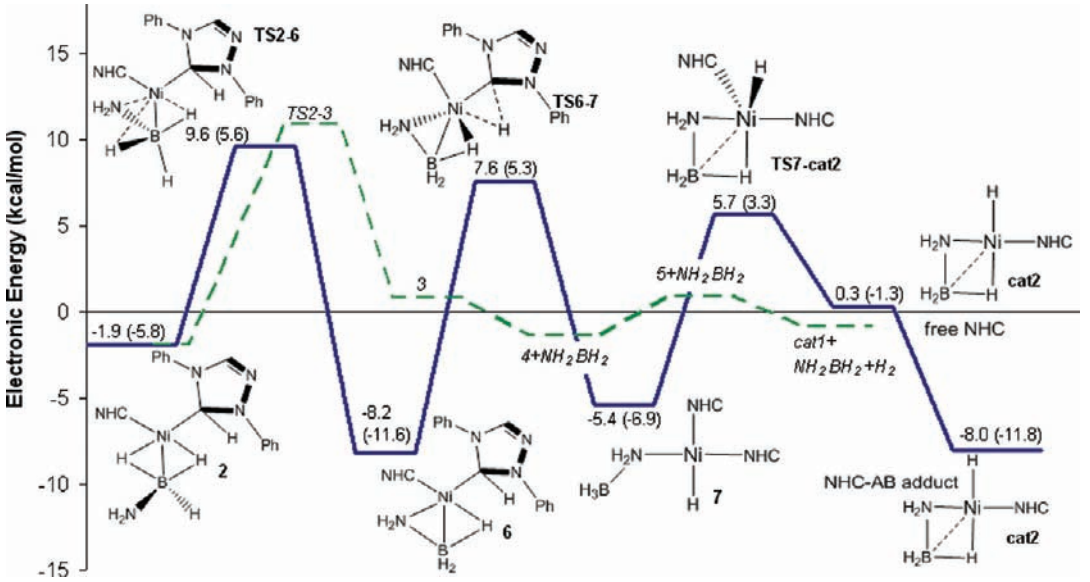

Figure 9. Pathway for **cat2** formation by NHC dissociation from **2** following **2**'s formation via **TS1**−**2** (Figure 2). This pathway is highly competitive with regeneration of **cat1** from **2**. Rate limiting barriers of competing pathways back to **cat1** are shown as horizontal lines. Formation of **cat2** releases **free NHC**, making it entropically favored over **cat1**. The released **free NHC** can then complex with **AB** to form the stable adduct **NHC-AB**. Not shown is the low barrier (15.1 kcal/mol (14.7 kcal/mol)) transformation of the **NHC-AB** adduct to form **NHC-(H)$_2$**, effectively preventing **free NHC** ligation to Ni.[14] The pathway returning to **cat1** from **2** is shown as a dashed line for comparison (see Figure 2).

both *cis* and *trans* conformations of the carbenes at the TS. The overall barrier for each cycle is shown in Table 2. Of these, the activation barrier nearest in energy to **TS1**−**2** is N−H activation (shown in the Supporting Information), which yields *cis*-Ni(NHC)$_2$(NH_2BH_3)(H) and has a barrier 6.3 kcal/mol (7.7 kcal/mol) larger than that of **TS1**−**2**. In addition to the higher barriers of these mechanisms, none show a significant B−H KIE, despite both B−H and N−H KIEs being observed experimentally, with the N−H KIE being stronger. Even though the 36.5 kcal/mol (35.9 kcal/mol) barrier for the dehydrogenation beginning with B−H activation makes it uncompetitive with **TS1**−**2**, its rate limiting step is proton elimination from the NH_3 of *cis*-Ni(NHC)$_2$$BH_2NH_3$(H), which greatly weakens the B−H KIE. These theoretical mechanisms yield B−H KIEs less than 1 because a d^{10} Ni(0) catalyst has no empty d orbitals for accepting a hydride; only after the proton has formally oxidized the metal to Ni(II) does a square planar coordination site become available and capable of accepting a hydride. In all rate-limiting steps, proton motion in the imaginary normal mode corresponding to the TS dominates over hydride motion. This is in contrast to the results we previously reported for an Ir pincer catalyst, which has HOMO and LUMO d-orbitals geometrically and energetically available for simultaneous acceptance of a proton and a hydride from **AB**.[4] Because none of the **cat1** dehydrogenation pathways yield a B−H KIE, alternate catalytically active species must be considered.

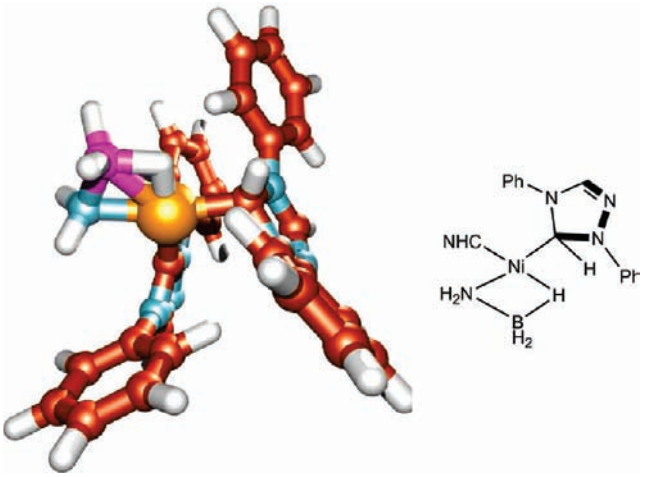

Figure 10. Reverse agostic complex **6**, formed as a result of facile isomerization of **2**, is an intermediate leading to NHC dissociation. The lowest barrier pathway following **AB** activation via **TS1−2** at **cat1** proceeds through **6** (See Figure 9).

NHC Dissociation from Ni(NHC)$_2$. Having exhausted the plausible **AB** activations at **cat1** without finding a pathway exhibiting the observed B−H KIE, we next examined pathways for generation of the alternative monocarbene catalytic species **cat2**. Although the activation of **AB** at **cat1** can regenerate **cat1**, dissociation of an NHC ligand from intermediate **2** of that cycle has a lower barrier than **AB** activation via **TS2−3** or **TS2−5** (see Scheme 2). This branch off the **cat1** cycle is illustrated in Figure 9 and begins with isomerization of **2** via **TS2−6** to form the agostic complex **6** (see Figure 10). **6** is similar to the isomerization intermediate **5** of the *cis*-carbene pathway, but with the NH_2BH_3 orientation reversed relative to the protonated carbene. The barrier to this isomerization is only 11.5 kcal/mol (11.5 kcal/mol), 3.1 kcal/mol (3.0 kcal/mol) lower than **TS2−5** and 1.3 kcal/mol (3.4 kcal/mol) lower than **TS2−3**. Intermediate **6** lies 2.3 kcal/mol (2.7 kcal/mol) higher in energy than **5** and undergoes C−H activation at its protonated carbene via **TS6−7** with a barrier 15.8 kcal/mol (16.9 kcal/mol) above **6**. **TS6−7** yields *cis*-Ni(NHC)$_2$(NH_2BH_3)(H) (**7**), shown in Figure 11, located 2.8 kcal/mol (4.7 kcal/mol) above **6**. The NH_2BH_3 group of **7** is attached to the Ni(II) center by the nitrogen lone pair and has an unassociated BH_3 group and a formal negative charge, making reaction of the BH_3 end with the Ni center likely.

From **7**, we identified two reaction pathways, each proceeding by reaction of the BH_3 end of NH_2BH_3: intramolecular B−H coordination to yield **3** and NHC displacement by the BH_3 end of NH_2BH_3 to yield **cat2**. B−H coordination of **7** to yield **3** involves a barrier 17.4 kcal/mol (16.6 kcal/mol) above **7**, while NHC displacement via **TS7-cat2** involves a barrier of 11.2 kcal/mol (10.2 kcal/mol). Consequently, NHC displacement is kinetically favored over B−H coordination by 6.2 kcal/mol (6.4 kcal/mol), and the kinetic products from reaction of **7** are **free NHC** and **cat2**. The **free NHC** lone pair can then associate with **AB** via an acidic hydrogen, forming an **NHC-AB adduct** 8.3 kcal/mol (10.5 kcal/mol) below separated **AB** and **free NHC**. The rate-limiting step for NHC displacement is **TS1−2**, (Figure 2) and **cat2** formation is kinetically favored over regeneration of **cat1** by

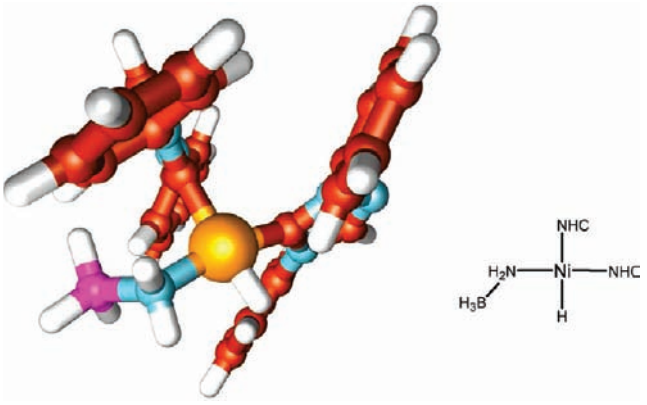

Figure 11. Intermediate **7** (*cis*-Ni(NHC)$_2$(NH_2BH_3)H), the product of C−H activation of **6** via **TS6−7**. The BH_3 end of NH_2BH_3 easily displaces an NHC to form **cat2**. The lowest barrier pathway following **AB** activation via **TS1−2** proceeds through **7** (See Figure 9).

1.3 kcal/mol (3.1 kcal/mol), although the difference is within the resolution of the theoretical approach. The pathway for transformation of **2** to **cat2** + **free NHC** is shown in Figure 9.

Not only is **cat2** formation kinetically favored, it is also thermodynamically favored as NHC displacement by **AB** is driven by mass action. This pathway establishes that **AB** displacement of NHC is a result of **AB** activation by **TS1−2**. Furthermore, because **cat2** + **NHC-AB adduct** is lower energy than **cat1** and the reverse reaction to yield **cat1** is enthalpically and entropically unfavorable, **cat2** represents a new energetic reference point for the system. Moreover, because **free NHC** can react with **AB** at relatively low barrier, 15.1 kcal/mol (14.7 kcal/mol) above the **NHC-AB adduct**, to produce **NHC-(H)$_2$** + NH_2BH_2, **free NHC** is not readily available to ligate to monocarbene catalyst species.[14] Because the energetic cost (neglecting entropy, which favors NHC dissociation) to regenerate **cat1** from **cat2** and **free NHC-AB adduct** is 18.9 kcal/mol (20.9 kcal/mol), formation of **NHC-(H)$_2$** is favored over formation of **cat1**.[14] Furthermore, **NHC-(H)$_2$** has two hydrogens attached to the carbene carbon, effectively deactivating **free NHC** as a potential ligand to Ni and making the reverse reaction to reform **cat1** virtually irreversible. Consequently, significantly more Ni catalyst will exist in the reaction media as monocarbene species **cat2** than as dicarbene species **cat1**.

Having shown that **cat2** formation is competitive with **AB** activation at **cat1** (Scheme 2), that **cat2** is thermodynamically favored over **cat1**, and is unlikely to revert to **cat1**, we now investigate the chemistry of **cat2**. We show that **cat2** does not dehydrogenate **AB** at any appreciable rate but instead transforms under experimental conditions into the monocarbene species **cat3**. Following the examination of **cat2**'s chemistry we then describe the catalytic activity of **cat3** along with potential routes for generating **cat2** from **cat3**.

Activation and Transformation of Ni(NHC)(NH_2BH_3)(H). The concentration of **cat2** is predicted to be significantly higher than that of **cat1** because **cat2** is thermodynamically favored over **cat1**, its formation is kinetically competitive after **AB** activation by **cat1** and **free NHC** transforms into **NHC-(H)$_2$** through facile reaction with **AB**, further driving equilibrium toward **cat2**. However,

Scheme 3. **AB** Does Not Facilely Activate at **cat2**, but **cat2** Can Transform into **cat3** by Reductive Elimination of H_2[a]

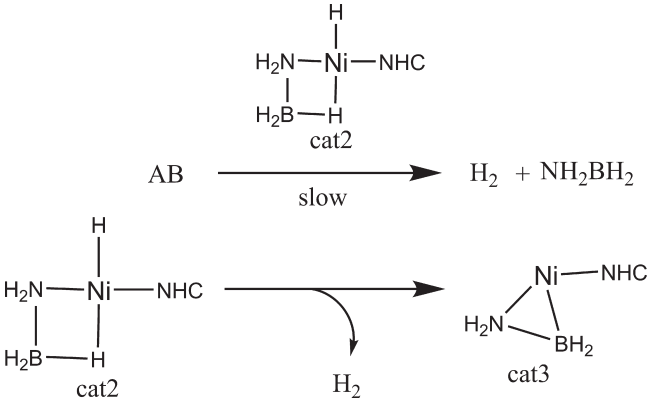

[a] This transformation is favorable because H_2 irreversibly bubbles out of the solvent. Transformation of **cat2** to **cat1** is also unfavorable because **cat2** is lower energy than **cat1** and **free NHC** is deactivated by reaction with **AB** to form NHC-$(H)_2$.

cat2 dehydrogenation of **AB** is not competitive because reaction of **AB** at **cat2** is shown to be relatively high barrier. Two reactions of **AB** at **cat2** are investigated and described next (see Scheme 3).

An acidic hydrogen from **AB** can associate favorably to a hydride on **cat2** to form **A** (see Supporting Information) with an energy 2.1 kcal/mol (4.8 kcal/mol) below the separated species. Because **cat2** is Ni(II), the *cis*-carbene mechanism analogous to **TS1−2** at **cat1**, which is Ni(0), is not possible, as Ni(II) has insufficient electron density available to donate to the carbene. In addition, B−H activation is not feasible because boron hydrides are unlikely to combine with Ni hydrides, and no available Ni coordination sites exist without oxidation to high energy Ni(IV). Instead, N−H activation or concerted activation (via **TSA-cat2**) of both types of **AB** hydrogens are more likely. N−H activation involves proton transfer from **AB** to the Ni-hydride closest to the **cat2** nitrogen. The products of N−H activation are free H_2 and NH_2BH_3 now attached to the Ni through a Ni−N bond (**7**). The barrier to this reaction lies 43.9 kcal/mol (43.8 kcal/mol) above **A**, making it uncompetitive at reaction conditions. Like N−H activation, concerted activation via **TSA-cat2** also involves proton transfer to the Ni hydride; however, a hydride from the boron end of **AB** simultaneously coordinates to Ni as shown in Figure 12, producing the agostic catalyst **cat2**, H_2, and NH_2BH_2. The barrier for **TSA-cat2** is 29.0 kcal/mol (28.0 kcal/mol) above **A**, indicating that activations of **AB** at the Ni(II) **cat2** will proceed through concerted activation but will be relatively slow. We note that **TSA-cat2** is similar to the concerted **AB** activation TS we reported for an Ir pincer catalyst.[4]

While **cat2** only activates **AB** with a relatively high barrier, it can release H_2 to yield **cat3** via two pathways as outlined in Scheme 4 and shown in Figures 13 and 14. Because the two hydrogens in **cat2** are *trans* to one another, both pathways involve isomerization to a *cis* conformation before reductive elimination of H_2 to generate **cat3**.

The first isomerization step of **cat2** is rotation of the NH_2BH_3 group to an η^2 complex (**C**) via **TScat2-C**. This

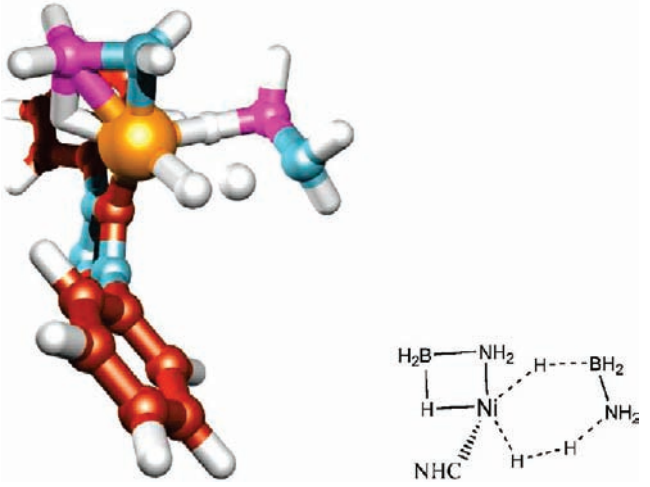

Figure 12. Transition state **TSA-cat2** for concerted activation of **AB** at **cat2**. Although this is the lowest energy **AB** activation at **cat2**, it is not kinetically competitive with **cat3** formation. Instead, **cat2** transforms to **cat3**, which does competitively activate **AB** (see Scheme 3).

Scheme 4. Pathways for **AB** Activation at Monocarbene **cat3**[a]

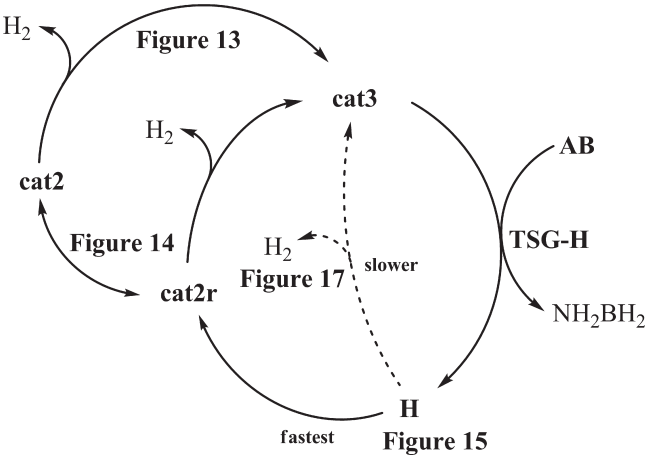

[a] Pathways include regeneration of **cat3** through **cat2r** (see Figures 13 and 14) and direct regeneration of **cat3** (less competitive and so illustrated here by a dashed line. See Figure 17 for details).

TS is similar to isomerization of **2** to **5** via **TS2−5** in the **cat1** *cis*-carbene pathway, where an additional B−H bond replaces the nitrogen lone pair donation to Ni (Figure 8). In both cases, the nitrogen lone pair donation is preferred energetically over the B−H sigma complex; in this case **C** is 9.6 kcal (9.7 kcal/mol) above **cat2** with the barrier for **TScat2-C** lying 25.4 kcal/mol (25.1 kcal/mol) above **cat2**. From **C**, a bridging hydrogen of the η^2 ligation combines with the Ni hydride through **TSC-D** to yield an H_2 adduct to the Ni along with NH_2BH_2 associated to Ni as a B−H sigma complex (**D**). **TSC-D** is slightly lower in energy than **D** because of its lower zero-point energy, although the electronic energy of **TSC-D** is slightly higher than that of **D** when the zero-point energy is excluded. After the formation of the H_2−Ni adduct **D**, the nitrogen of NH_2BH_2 can reassociate to the metal center through **TSD-E**. This yields **E**, a **cat3**-H_2 adduct with H_2 attached near the nitrogen end of NH_2BH_2. From **E**, H_2 dissociates to yield **cat3** with a barrier of 3.4 kcal/mol (3.6 kcal/mol), and the products are

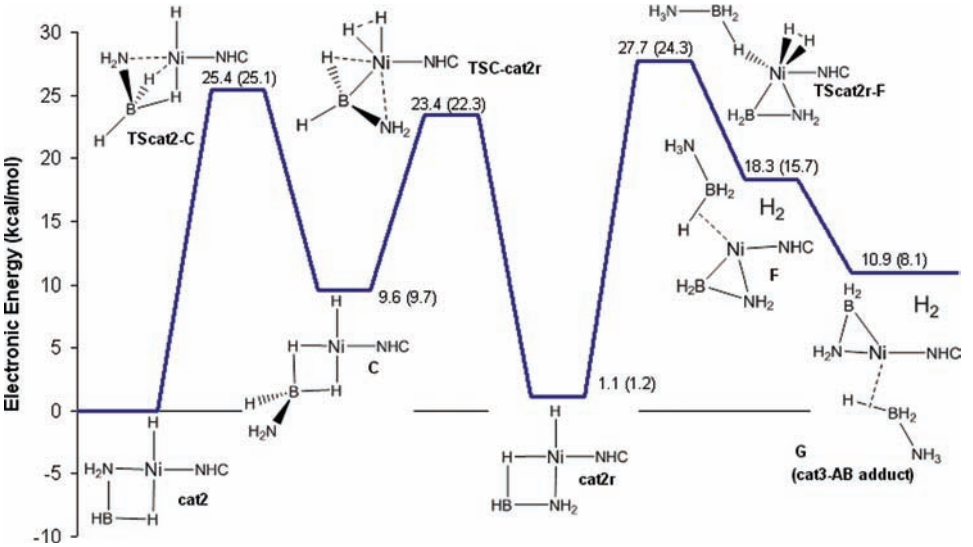

Figure 13. Electronic energy diagram for reductive elimination of H_2 from **cat2** to yield **cat3**. This pathway exhibits both N−H and B−H KIE in the rate limiting steps. Because the released H_2 bubbles out of solution, this path is only reversible in the presence of additional H_2. ΔG^{333K} for **cat2** → **cat3** + H_2 is 6.0 kcal/mol (5.4 kcal/mol).

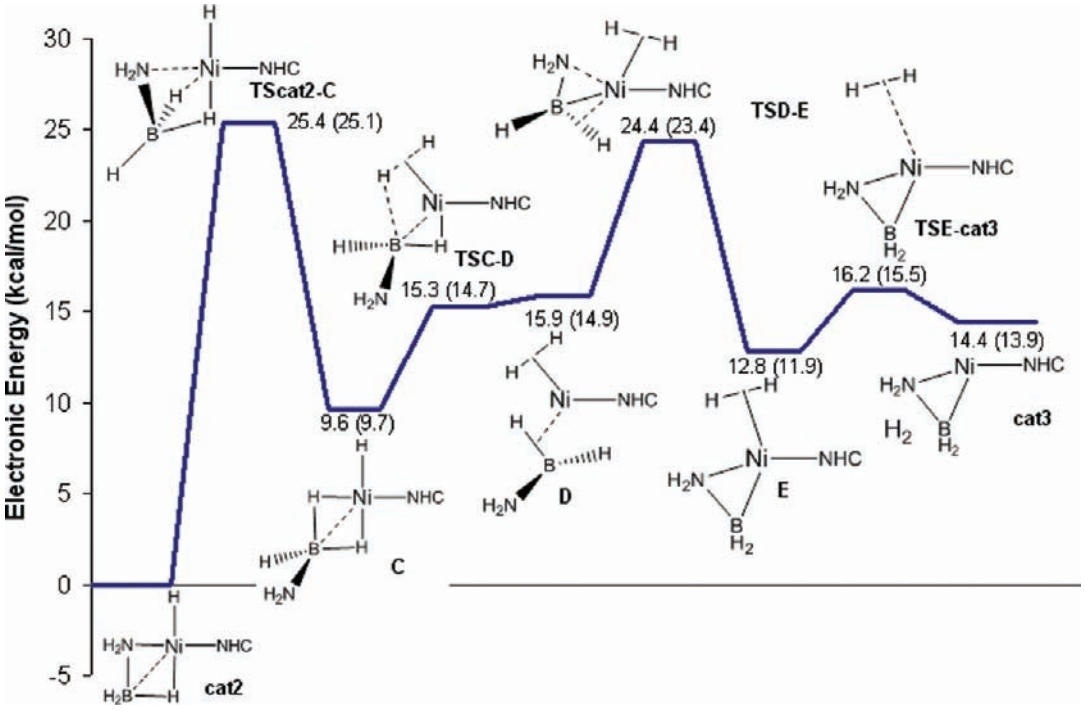

Figure 14. Alternative electronic energy diagram for pathway connecting **cat2** to **cat3** (the **cat3-AB** adducts are isomers **F** and **G**, where **G** is produced by simple dissociation and reassociation of **AB** to **cat3**) proceeding through **AB** displacement of H_2. This pathway is similar in overall barrier to the pathway in Figure 13.

1.7 kcal/mol (2.0 kcal/mol) above **E**. The rate limiting barriers are **TScat2-C** and **TSD-E**, each of which contains both N−H and B−H KIE with **TScat2-C** giving ND_3BH_3, 1.5; NH_3BD_3, 1.1; ND_3BD_3, 1.5 and **TSD-E** giving ND_3BH_3, 1.3; NH_3BD_3, 1.7; ND_3BD_3, 2.0. These transition states both contain significant R-H motion in the vibrational mode corresponding to the reaction coordinate, producing a KIE without bond breaking. Although this KIE is not a result of direct **AB** dehydrogenation, it does affect the rate of formation of **cat3**. Also, despite the total energy for **cat2** → **cat3** + H_2 being 14.4 kcal/mol (13.9 kcal/mol) endothermic, the overall free energy at 60 °C for this reaction is only 6.0 kcal/mol (5.4 kcal/mol) uphill taking into account the release of hydrogen gas from the system. Furthermore, because the experimental system releases H_2 gas, the generation of **cat3** is irreversible.

An alternative pathway for formation of **cat3** from **cat2** is shown in Figure 14. This pathway produces **cat3** by displacement of H_2 from **cat2** and involves a similar barrier to that of reductive elimination shown in Figure 13. The first step, **TScat2-C**, is the same as in the previous pathway via **TScat2-C**. Following formation of **C**, a second isomerization (**TSC-cat2r**) occurs to reform the nitrogen lone pair coordination with the metal. The path through this TS forms an agostic complex

(**cat2r**) with the B−H and N positions interchanged relative to **cat2** and involves a barrier of 13.8 kcal/mol (12.7 kcal/mol). **cat2r** is expected to have similar reactivity with **AB** to **cat2** and is nearly isoenergetic to **cat2** being only 1.1 kcal/mol (1.2 kcal/mol) higher in energy. From **cat2r**, an **AB** from solution can displace H_2 via **TScat2r-F** with a barrier 27.7 kcal/mol (24.3 kcal/mol) above **cat2** to yield the **cat3-AB** adduct **F** with **AB** attached to Ni as a B−H sigma complex cis to the BH_2 of the NH_2BH_2 ligand. **F** lies 18.3 kcal/mol (15.7 kcal/mol) above **cat2**. Since **F** is not the lowest energy complex of **AB** with **cat3**, it can undergo simple dissociation and reassociation of **AB** to yield **G**, a lower energy **AB-cat3** adduct (vide infra). The rate of this second pathway for transformation of **cat2** to **cat3** is determined by the overall rate of surmounting **TScat2r-F**, which has a barrier of 27.7 kcal/mol (24.3 kcal/mol), similar to **TScat2-C**. **TScat2r-F** also contains both N−H and B−H KIE (ND_3BH_3, 1.4; NH_3BD_3, 1.8; ND_3BD_3, 2.2). Again, although this pathway is endothermic, the system is open and the reaction was studied under non-equilibrium conditions that make the transformation essentially irreversible.

The simplified scheme proposed in Scheme 1 indicates that only **cat1** and **cat3** can competitively dehydrogenate **AB**, while **cat2** is a key intermediate that can transform into **cat3** and also be regenerated. Having described the activation of **AB** by **cat1**, **cat1**'s transformation into **cat2** and **cat2**'s inability to competitively dehydrogenate **AB**, we next study the chemistry of **cat3**. While only N−H isotope effects exist for activation of **AB** through **cat1**, both N−H and B−H KIEs are present through consideration of the full catalytic cycle, including Ni monocarbene complexes.

Chemistry of Ni(NHC)(NH_2BH_2). The aminoborane analogue to ethylene-Ni complexes, **cat3**, is highly active in dehydrogenating **AB**. Because in **cat3** NH_2BH_2 replaces one NHC of **cat1**, **cat3** may activate **AB** differently than **cat1** because of both steric and electronic factors. However, **cat1** and **cat3** are both Ni(0) species with open coordination sites. Thus, an **AB** activation mechanism proceeding through a transition state analogous to **TS1−2** is competitive at **cat3**. Table 3 lists the predicted overall barriers for several possible mechanisms at **cat3**. *trans* activations were not studied because of their significantly higher barriers for **cat1**, which are also expected to be high for **cat3**. The energetic ordering of the activations at **cat3** is similar to **cat1**, and the most favorable pathway for **AB** dehydrogenation at **cat3** is the *cis*-carbene mechanism via **TSG-H** (Figure 15) analogous to **TS1−2**. The *cis* concerted mechanism, **TS1−4** favored at Imes **cat1** is also possible at **cat3**. Similar to **cat1**, B−H activation of **AB** at **cat3** has a high overall barrier, eliminating the possibility that it accounts for the observed B−H KIE. The rate-limiting step of **AB** dehydrogenation beginning with B−H activation involves proton elimination following the B−H activation.

Similar to **cat1**, **cat3** can associate with **AB** to yield either an N−H adduct or a B−H sigma complex. Because NHC are strong donors, monocarbene complexes are

Table 3. Activation Energies for the Rate Limiting Step of Different **AB** Activation Pathways at **cat3**[a]

	rate limiting barrier	
AB activation type	*E*(THF)	*E*(Benzene)
cis carbene assisted activation (**TSG-H**)	21.1	19.8
cis concerted activation	26.2	24.7
cis N−H activation	27.2	26.7
cis B−H activation[b]	30.6	29.4

[a] As with **cat1**, the *cis*-carbene activation mechanism is favored. [b] The barrier for *cis* B−H activation is the result of a proton elimination barrier to complete the cycle.

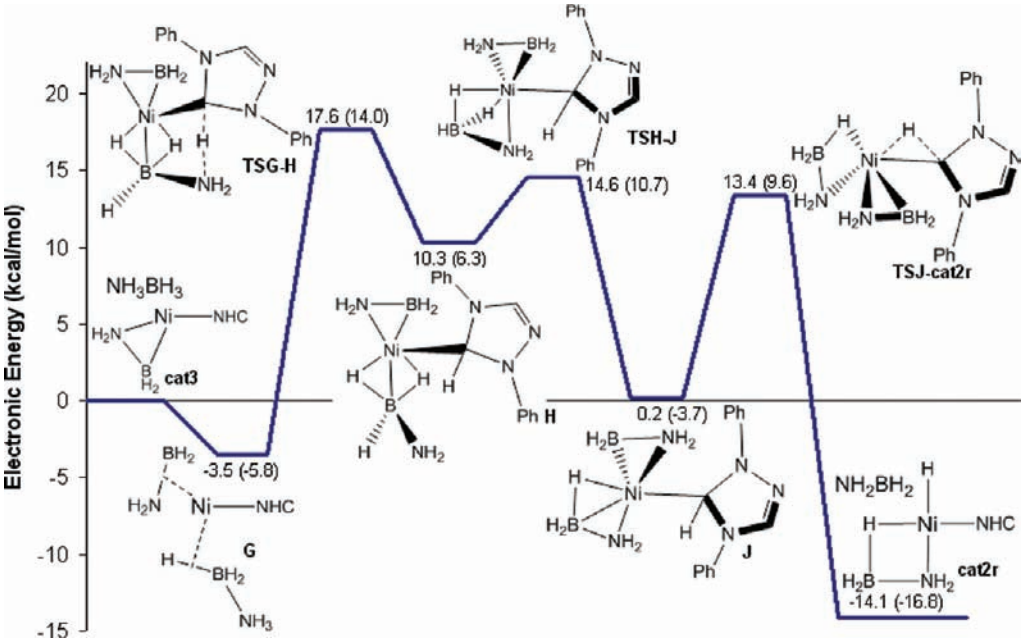

Figure 15. Lowest energy pathway for activation of **AB** by **cat3** where *cis*-carbene assists the activation by accepting an N−H proton of **AB** in **TSG-H**, similar to **TS1−2** at **cat1**. This pathway results in formation of **cat2r** and release of NH_2BH_2. Transformation of **cat2r** into **cat3** and release of H_2 is described in Scheme 4 and Figure 17.

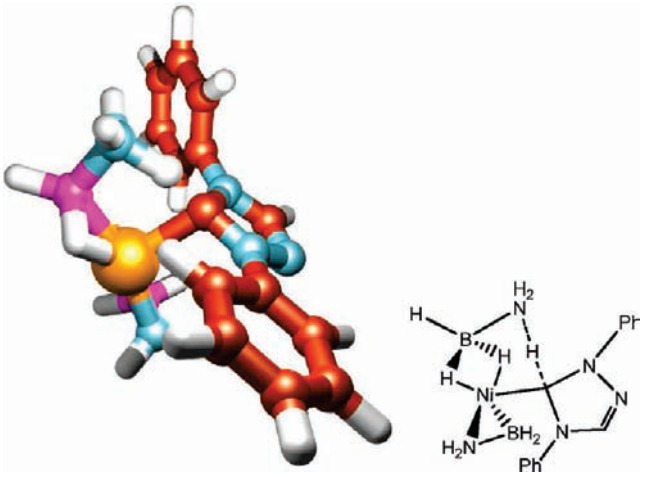

Figure 16. Transition state **TSG-H** for **AB** activation at **cat3** via the *cis*-carbene mechanism. Note that this structure is nearly square pyramidal with the carbene in an apical position. See Scheme 4 for an overview of the reactions following **TSG-H** and Figures 15 and 17 for the energetics of the **AB** activation pathway through **TSG-H**.

expected to have significantly lower charge density on the Ni than dicarbene complexes. Thus, Ni-monocarbene should have a less favorable interaction between acidic hydrogens of **AB** and the Ni. This is indeed the case, as N−H association to **cat3** is favorable over separated **AB** and **cat3** by only 2.4 kcal/mol (5.0 kcal/mol). Instead, a B−H sigma complex formed *cis* to the NH_2BH_2 nitrogen of **cat3** (**G**) is slightly more favorable, 3.5 kcal/mol (5.8 kcal/mol) below the separated species.

***cis*-Carbene Activation at Ni(NHC)(NH_2BH_2).** *cis*-Carbene activation of **AB** at **cat3** proceeds through a single rate limiting step (**TSG-H**) but then branches into two pathways. The pathways for *cis*-carbene activation of **AB** to regenerate **cat3** are summarized in Scheme 4, and described in detail below. Figure 15 shows the lower barrier pathway, which results in **cat2r** formation. **cat2r** transforms into either **cat2** or **cat3**, as shown in Figure 14. Alternatively to **cat2r** production after **TSG-H**, direct regeneration of **cat3** can occur as shown in Figure 17.

The lowest barrier pathway for activation of **AB** at **cat3** is shown in Figure 15 and proceeds through **TSG-H** (Figure 16). **TSG-H** involves proton transfer from **AB** to the *cis*-carbene concomitant with B−H ligation to the metal analogous to **TS1−2** at **cat1**. Because the Ni center has only one carbene ligand, a larger amount of charge donation from **AB**'s hydrides to Ni is required to compensate for the lower donation of the single carbene relative to that of the two carbenes of **cat1**. This effect causes η^2 H−B−H ligation to Ni at the TS, with two B−H bonds donating to the Ni center. The η^2 H−B−H ligation of BH_3 is nearly planar with the NH_2BH_2 *trans* to **AB**. The TS thus forms a nearly square pyramidal Ni with the carbene forming the top of the pyramid. It is apparent from this geometry that **TSG-H** is not entirely analogous to **TS1−2**. Here, the square pyramidal geometry of **TSG-H** allows the carbene to receive electron donation via the Ni d_{z^2} orbital, accessible from the open apical position above the square planar base. In contrast, the preferred geometry of the square planar base in **TSG-H** is inaccessible in **TS1−2** because the steric bulk of the carbenes preclude this structure. While η^2 ligation of H−B−H has the effect of sterically allowing only one NHC phenyl to be coplanar with the central 5-membered ring, this stabilizes the extended delocalization sufficiently for **TSG-H** to be only 21.1 kcal/mol (19.8 kcal/mol) above **G**, which is slightly lower in energy than *cis*-carbene activation through **TS1−2**. **TSG-H** only contains an N−H KIE (ND_3BH_3, 4.2; NH_3BD_3: 1.0; ND_3BD_3, 4.3).

Completing the *cis*-Carbene Activation Cycle at Ni(NHC)(NH_2BH_2). We examine two pathways that complete the *cis*-carbene activation cycle at **cat3** following the formation of intermediate **H**. The more kinetically competitive of the two results in the production of **cat2r** (see Figure 15). We first describe a less competitive path shown in Figure 17 that regenerates **cat3** directly (see Scheme 4). Intermediate **H** produced by **TSG-H** is analogous to **2** in the **cat1** *cis*-carbene mechanism and involves η^2 association of H−B−H of **AB** to Ni and a proton attached to the carbene carbon. However, like **2**, **H** is relatively unstable lying 13.8 kcal/mol (12.1 kcal/mol) above the B−H sigma complex **G**. This indicates that more favorable isomers of **H** with the nitrogen lone pair donated to the metal likely exist. Following an analogous mechanism to the *cis*-carbene pathway of Figure 2, direct C−H activation of the carbene proton (**TSH-E**) can occur with an energetic cost of 21.4 kcal/mol (20.4 kcal/mol) above **G**. The product (**E**) of this activation is free NH_2BH_2 and H_2 attached to the Ni catalyst, which can be released via H_2 elimination through **TSE-cat3** to regenerate **cat3**.

Although **TSH-E** is roughly equivalent in barrier to **TSG-H**, isomerization of **H** to the agostic species **J** through **TSH-J** is favored (see Figure 17 and Scheme 4), with a barrier 18.1 kcal/mol (16.5 kcal/mol) above **G**. **J** involves nitrogen lone pair donation to Ni and one hydride from BH_3 participating in an agostic interaction with Ni, making it 10.1 kcal/mol (10.0 kcal/mol) more stable than **H**. Then, C−H activation through **TSJ-cat2r** occurs with a barrier 13.2 kcal/mol (13.3 kcal/mol) above **J**. An IRC analysis shows the products of **TSJ-cat2r** are **cat2r** and free NH_2BH_2. Overall, the dehydrogenation of **AB** by **cat3** resulting in free NH_2BH_2 and **cat2r** has a rate-limiting barrier of 21.1 kcal/mol (19.8 kcal/mol) and is exothermic by 10.6 kcal/mol (11.1 kcal/mol). The competitive pathway (Figure 17) through **TSH-E** has an overall barrier of 21.4 kcal/mol (20.4 kcal/mol) and regenerates **cat3** through release of NH_2BH_2 and H_2. Because both pathways proceed through **TSG-H**, the competition between **TSH-J** and **TSH-E** determines whether **cat2r** or **cat3** is formed after *cis*-carbene activation. **TSH-J** is energetically favored over **TSH-E** by 3.3 kcal/mol (3.9 kcal/mol) and thus **cat2r** is predicted to be the major product after **AB** activation at **cat3**. Since **cat2r** formation is favored, **cat3** must be regenerated before further **AB** activation occurs. Scheme 4 shows the transformations of **cat2r** to **cat3**, which are rate-limiting and exhibit both N−H and B−H KIE, as previously described. Therefore **AB** activation by **cat3** shows both N−H and B−H KIE, in accordance with experimental observations for the active catalyst.[7]

Discussion

This study investigates numerous **AB** dehydrogenation pathways in the Ni model Enders' carbene system to provide

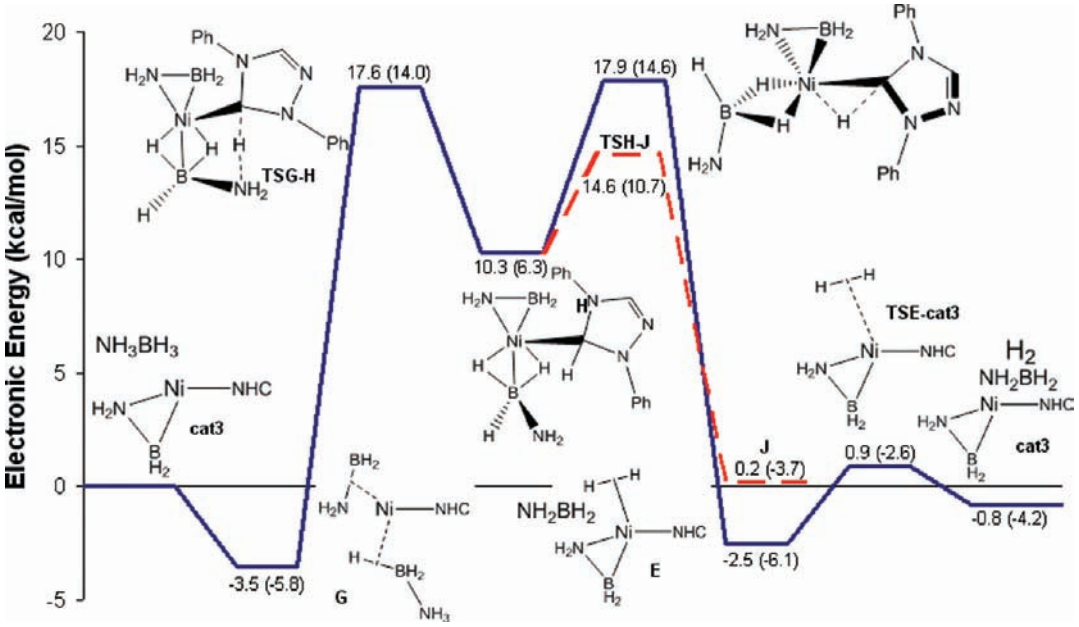

Figure 17. Alternative pathway to transform **H** back into **cat3** following **TSG-H** (Figure 16). The dashed line represents the energy of the more favorable, competing pathway leading to **cat2r** through **TSH-J**.

a detailed description of the reaction mechanism and associated energetics, and to explain experimental observations. While $Ni(NHC)_2$ was previously assumed to be the primary active catalyst, [10] a thorough examination of reactions at $Ni(NHC)_2$ show that its reactivity cannot explain experiment and that it competitively transforms to monocarbene species. For example, activation of **AB** by the *cis*-carbene mechanism of **cat1** contains only N−H KIE, as previously predicted for this same catalyst. [see Supporting Information of ref 10] Because **AB** dehydrogenation by **cat1** does not contain a B−H KIE, it cannot fully explain the experimental kinetics. On the other hand, catalyzed **AB** dehydrogenation at monocarbene Ni complexes fully account for the experimental observations, including the presence of both N−H and B−H KIE, the observation of NHC-BH_3, the experimental temperature, as well as being favored kinetically and thermodynamically under the non-equilibrium conditions of the open system. Furthermore, the monocarbene catalyst has an AB-derived ligand, which is strongly supported by NH_2BH_2 trapping experiments where NH_2BH_2 is observed to remain attached to the Ni NHC catalyst at 25 °C.[13] Because **AB** activation is lower barrier than the rate limiting steps leading to NH_2BH_2 release, **AB** can attach to Ni at a lower temperature than NH_2BH_2 will be released. These results[13] support **cat2** as the most favorable product after **AB** activation by **cat1**.

We show that the *cis*-carbene mechanism, which involves **AB** proton transfer to the carbene, strongly depends on delocalization factors, where broken aromaticity is stabilized by coplanar phenyl rings. Our results show that the *cis*-carbene mechanism is not active with the Imes NHC catalyst because the methyl groups on the Imes phenyl rings prevent them from becoming coplanar and stabilizing the broken aromaticity of the carbene.

Scheme 1 shows the lowest barrier pathways for **AB** dehydrogenation. We note that although **cat1** can dehydrogenate **AB** catalytically, dehydrogenation must compete with NHC dissociation leading to **cat2**, with NHC dissociation being kinetically favored by 1.3 kcal/mol (3.1 kcal/mol). For this reason, **cat2** quickly forms in the reaction media with the rate of production proportional to the rate of **AB** dehydrogenation. **cat2** formation is not only favored kinetically after **AB** activation (**TS1−2**) at **cat1**, it is also lower in energy and higher in entropy than **cat1** because of carbene dissociation. Furthermore, regeneration of **cat1** by the reverse reaction—NHC association to **2**—is unfavorable because **free NHC** reacts with abundant **AB** and a low barrier to yield inactive NHC-$(H)_2$.[14] Furthermore, because the N−B bond of **AB** is relatively weak,[33] a small amount of free NH_3 and BH_3 will exist in the reaction media. We calculate that BH_3 associates to **free NHC** without barrier to yield the experimentally observed NHC-BH_3 adduct,[7] further supporting the predicted displacement of NHC by **AB**.

While the monocarbene species **cat2** formed from **cat1** cannot activate **AB** at a competitive rate, it does transform into **cat3**, which activates **AB** with overall barriers consistent with experiment. Although **cat3** formation is uphill energetically, it is essentially irreversible because the reaction is run under open conditions, as H_2 continuously bubbles out of the system, lowering the free energy of **cat3**. The primary mechanism of **AB** dehydrogenation (Figure 15) is through a *cis*-carbene activation pathway that produces **cat2r**, which releases H_2 to regenerate **cat3**. An alternative branch of this mechanism regenerates **cat3** directly (Figure 17) but involves a barrier 3.3 kcal/mol (3.9 kcal/mol) higher than that of **cat3** regeneration through **cat2r**.

The rate of **AB** dehydrogenation therefore depends on the dynamic local equilibrium between **free NHC**, **cat1**, **cat2**, **cat2r**, **cat3**, and H_2 as represented in Scheme 1. We again emphasize that the removal of H_2 from the system makes production of **cat3** through release of H_2 irreversible. The two lowest barrier **AB** activations occur at **cat1** and **cat3**, and the activations result in production of **cat2** and **cat2r**, respectively. The transformation of **cat1** and **cat3** into species that

(33) Dixon, D. A.; Gutowski, M. *J. Phys. Chem. A* **2005**, *109*, 5129.

do not directly activate **AB** indicates that the rate of **AB** dehydrogenation is limited by elimination of H_2 from **cat2** and its isomer **cat2r**. The slowest active pathways in the local dynamic equilibrium between **free NHC**, **cat1**, **cat2**, **cat2r**, and **cat3** are elimination of H_2 from **cat2** and **cat2r** to yield **cat3**, with rate limiting barriers as shown in Scheme 4. These rate-limiting mechanisms each exhibit both B−H and N−H KIEs, and although they are not activations of **AB**, they do govern the overall rate of reaction and thus the disappearance of **AB**.

The rate limiting barriers of about 22−25 kcal/mol are consistent with the experimental conditions that required heating to 60 °C to achieve a reasonable rate of reaction. These barriers are higher than the 20.7 kcal/mol overall energetic barrier for activation of **AB** at an Ir pincer catalyst,[4] as expected because the Ir catalyst dehydrogenated **AB** quickly at room temperature. The rate limiting steps of **AB** activation contain the experimentally observed KIE for both types of **AB** hydrogen. The criteria for N−H or B−H KIE are significant motion of N−H or B−H hydrogen in the normal mode corresponding to the transition state. This can occur without N−H or B−H bond dissociation, although bond breaking generally shows higher KIEs. The rate limiting steps show a strong N−H KIE in the *cis*-carbene activations at **cat1** (ND_3BH_3, 4.6; NH_3BD_3, 0.8; ND_3BD_3, 3.9) and **cat3** (ND_3BH_3, 4.2; NH_3BD_3, 1.0; ND_3BD_3, 4.3), as well as combined N−H and B−H KIE for H_2 elimination from **cat2** (ND_3BH_3, 1.3; NH_3BD_3, 1.7; ND_3BD_3, 2.0) and **cat2r** (ND_3BH_3, 1.4; NH_3BD_3, 1.8; ND_3BD_3, 2.2). Because the *cis*-carbene activations are faster than H_2 elimination, the calculated N−H KIE in the *cis*-carbene steps are higher than would be realized experimentally. Overall, the predicted KIE for the *cis*-carbene activation to H_2 elimination cycle is in excellent agreement with the experimental KIE (ND_3BH_3, 2.3; NH_3BD_3, 1.7; ND_3BD_3, 3.0). Because the B−H KIE is only predicted with consideration of elimination of H_2 from **cat2** and **cat2r**, the overall pathway for catalytic dehydrogenation of **AB** can be adequately described in terms of the monocarbene Ni species.

Conclusion

This study provides a detailed description of the reactions of **AB** at Ni carbene catalysts, and by considering reactions at monocarbene Ni species **cat2** and **cat3**, accounts for the observed combined N−H and B−H KIE and rate of **AB** dehydrogenation. Monocarbene species are energetically, kinetically, and entropically favored over dicarbene species following activation of **AB** at the dicarbene Ni catalyst **cat1**. Our results show that the barrier to transform the dicarbene species **2** (which results from the activation of **AB** at **cat1**) back to **cat1** is 1.3 kcal/mol (3.1 kcal/mol) higher than its conversion to the monocarbene species **cat2** (with release of **free NHC**). Furthermore, reaction of **free NHC** with abundant **AB** or BH_3 significantly favors the monocarbene catalyst. [14] The predicted barriers for the rate limiting steps of 22−25 kcal/mol are consistent with the experimental conditions that required heating to 60 °C to achieve a reasonable rate of reaction.

Electron delocalization is a governing factor in the ability of Ni carbenes to dehydrogenate **AB**. We show that the degree to which the steric demands of the ligands allow electron delocalization between the Ni center and the carbenes determines what types of carbene ligands (Enders' carbene, but not Imes or Idipp) are able to facilitate the *cis*-carbene mechanism at both mono and dicarbene Ni. Furthermore, the many different associations of partly dehydrogenated **AB** species to Ni suggest the need to account for multiple isomers when investigating the reactivity of **AB** at organometallic complexes because these isomers are important intermediates that determine whether the NHC ligands remain bound during the catalytic cycle.

Although this system experimentally removed ∼2.5 equiv of H_2 from **AB**, this investigation only considers removal of the first equivalent where NH_2BH_2 and $(NH_2BH_2)_n$ concentrations are low compared to **AB**. Removal of the second and third equivalents of H_2 might also occur with the same mechanisms and catalytic species presented here, and our other study addresses those aspects of this system.[14] The various important aminoborane oligomers necessary to account for the removal of the second equivalent of H_2 from **AB** have been discussed in the literature [2,34] and studied by our group.[35] Our results suggest that the small steric bulk of **cat3** may provide an avenue for dehydrogenation of bulky oligomeric $(NH_2BH_2)_n$ species. A final consideration to be addressed in future work is how the fuel-cell poison borazine is removed by cross-linking, which may also be feasible at **cat3**.

Supporting Information Available: Additional information as noted in the text. This material is available free of charge via the Internet at http://pubs.acs.org.

(34) Marder, T. B. *Angew. Chem., Int. Ed.* **2007**, *46*(43), 8116–8118.
(35) Zimmerman, P. M.; Paul, A.; Zhang, Z.; Musgrave, C. B. *Inorg. Chem.* **2009**, *48*(3), 1069–1081.